**Your Safety • Your Mobility
Your Economic Opportunity**

RP 256

Fatigue Crack Detection Using Unmanned Aerial Systems in Under-Bridge Inspection

By
Sattar Dorafshan
Marc Maguire
Nathan V. Hoffer
Calvin Coopmans

Department of Civil and Environmental Engineering
Utah State University

Prepared for
Idaho Transportation Department
Research Program, Contracting Services
Division of Engineering Services
http://itd.idaho.gov/alt-programs/?target=research-program

August 2017

1. Report No. FHWA-ITD-17-256	2. Government Accession No.	3. Recipient's Catalog No.
4. Title and Subtitle Fatigue Crack Detection Using Unmanned Aerial Systems in Under-Bridge Inspection		5. Report Date August 2017
		6. Performing Organization Code
7. Author(s) Sattar Dorafshan, Marc Maguire, Nathan V. Hoffer, Calvin Coopmans		8. Performing Organization Report No.
9. Performing Organization Name and Address Department of Civil and Environmental Engineering Utah State University 4110 Old Main Hill Logan, UT 84322		10. Work Unit No. (TRAIS)
		11. Contract or Grant No. USU-2016-01
12. Sponsoring Agency Name and Address Idaho Transportation Department Division of Engineering Services, Contracting Services, Research Program PO Box 7129 Boise, ID 83707-7129		13. Type of Report and Period Covered Final Report 02/01/2016 - 1/31/2017
		14. Sponsoring Agency Code RP 256

15. Supplementary Notes

Project performed in cooperation with the Idaho Transportation Department and FHWA.

16. Abstract

The applications of Unmanned Aerial Systems (UAS) for bridge inspection, with emphasis on under-bridge inspection and fatigue crack detection, were studied in this report. The potential benefits and challenges of using UAS for bridge inspection were identified through an extensive literature survey. The feasibility of using UAS for fatigue crack detection was studied by determining the minimum lighting, camera distance and environmental requirements for three UAS. The DJI Mavic UAS performed better than the others in both indoor and outdoor GPS-denied inspections. An in-service bridge in Ashton, Idaho was inspected using this UAS to find fatigue cracks. No fatigue crack, known or new, was detected in the UAS images but marker lines around the known fatigue cracks (drawn by the inspectors in previous inspections), concrete defects, and steel rust were detected. Thermography showed promising results for fatigue crack detection in a lab setting, but it was not feasible for UAS applications since it had to be performed using active thermography techniques to obtain adequate results. Additionally, image processing algorithms for autonomous detection of both concrete and fatigue cracks were successfully developed. These algorithms, especially for fatigue crack detection, require more images to perform better, but were demonstrated as feasible to aid in a real-time inspection.

17. Key Words Unmanned Aerial Vehicles, Unmanned Aerial Systems, Bridge Inspection, Fatigue Cracks, Concrete Cracks, Bridge Condition Assessment, Remote Sensing, Thermography, Image Processing, Fracture Critical Bridge Inspection.	18. Distribution Statement Copies available online at http://itd.idaho.gov/alt-programs/?target=research-program

19. Security Classification (of this report) Unclassified	20. Security Classification (of this page) Unclassified	21. No. of Pages 120	22. Price None

METRIC (SI*) CONVERSION FACTORS

APPROXIMATE CONVERSIONS TO SI UNITS

Symbol	When You Know	Multiply By	To Find	Symbol
		LENGTH		
in	inches	25.4		mm
ft	feet	0.3048		m
yd	yards	0.914		m
mi	Miles (statute)	1.61		km
		AREA		
in^2	square inches	645.2	millimeters squared	cm^2
ft^2	square feet	0.0929	meters squared	m^2
yd^2	square yards	0.836	meters squared	m^2
mi^2	square miles	2.59	kilometers squared	km^2
ac	acres	0.4046	hectares	ha
		MASS (weight)		
oz	Ounces (avdp)	28.35	grams	g
lb	Pounds (avdp)	0.454	kilograms	kg
T	Short tons (2000 lb)	0.907	megagrams	mg
		VOLUME		
fl oz	fluid ounces (US)	29.57	milliliters	mL
gal	Gallons (liq)	3.785	liters	liters
ft^3	cubic feet	0.0283	meters cubed	m^3
yd^3	cubic yards	0.765	meters cubed	m^3

Note: Volumes greater than 1000 L shall be shown in m^3

Symbol	When You Know	Multiply By	To Find	Symbol
		TEMPERATURE (exact)		
^oF	Fahrenheit temperature	5/9 (^oF-32)	Celsius temperature	^oC
		ILLUMINATION		
fc	Foot-candles	10.76	lux	lx
fl	foot-lamberts	3.426	candela/m^2	cd/cm^2
		FORCE and PRESSURE or STRESS		
lbf	pound-force	4.45	newtons	N
psi	pound-force per square inch	6.89	kilopascals	kPa

APPROXIMATE CONVERSIONS FROM SI UNITS

Symbol	When You Know	Multiply By	To Find	Symbol
		LENGTH		
mm	millimeters	0.039	inches	in
m	meters	3.28	feet	ft
m	meters	1.09	yards	yd
km	kilometers	0.621	Miles (statute)	mi
		AREA		
mm^2	millimeters squared	0.0016	square inches	in^2
m^2	meters squared	10.764	square feet	ft^2
km^2	kilometers squared	0.39	square miles	mi^2
ha	hectares (10,000 m^2)	2.471	acres	ac
		MASS (weight)		
g	grams	0.0353	Ounces (avdp)	oz
kg	kilograms	2.205	Pounds (avdp)	lb
mg	megagrams (1000 kg)	1.103	short tons	T
		VOLUME		
mL	milliliters	0.034	fluid ounces (US)	fl oz
liters	liters	0.264	Gallons (liq)	gal
m^3	meters cubed	35.315	cubic feet	ft^3
m^3	meters cubed	1.308	cubic yards	yd^3

Symbol	When You Know	Multiply By	To Find	Symbol
		TEMPERATURE (exact)		
^oC	Celsius temperature	9/5 ^oC+32	Fahrenheit temperature	^oF
		ILLUMINATION		
lx	lux	0.0929	foot-candles	fc
cd/cm^2	candela/m^2	0.2919	foot-lamberts	fl
		FORCE and PRESSURE or STRESS		
N	newtons	0.225	pound-force	lbf
kPa	kilopascals	0.145	pound-force per square inch	psi

Acknowledgements

Technical Advisory Committee

Each research project is supervised by a technical advisory committee (TAC), led by an ITD project sponsor and project manager. The Technical Advisory Committee (TAC) is in charge of overseeing the project progress, reviewing deliverables and ensuring that study objectives are met in a timely manner. The work of the following TAC members in guiding this research study is gratefully recognized.

Project Sponsor – Matt Farrar, PE, State Bridge Engineer

Project Manager – Dan Gorley, PE, Bridge Asset Management Engineer

TAC Members

Alan Buehrig, PE

Mike Pape

James Bennett

FHWA-Project Advisor — Ed Miltner, PE

Table of Contents

List of Tables

List of Figures

List of Acronyms

AASHTO	American Association of State Highway and Transportation Officials
AS	Altitude Sensor
COA	Certificate of Authorization
DOT	Department of Transportation
FAA	Federal Aviation Administration
FCM	Fracture Critical Member
FDOT	Florida Department of Transportation
FHWA	Federal Highway Administration
FL	Flight Level
FPV	First Person View
GPS	Global Positioning System
IFR	Instrument Flight Rules
INS	Inertial Navigation Sensors
ITD	Idaho Transportation Department
LiDAR	Light Detection and Ranging
LoG	Laplacian of Gaussian
MEMs	Micro-Electro-Mechanical System
MP	Mega-Pixel
MSL	Mean Sea Level
NBI	National Bridge Inventory
NDE	Non-Destructive Evaluation
SLAM	Simultaneous Localization and Mapping
SMASH Lab	Systems, Materials, and Structural Health Lab
TSA	Transportation Safety Administration
UAS	Unmanned Aerial System
AUVSI	Association for Unmanned Vehicle Systems International
UBIT	Under Bridge Inspection Truck
UWRL	Utah Water Research Laboratory
VFR	Visual Flight Rules
VTOL	Vertical Take-Off and Landing

Executive Summary

The Idaho Transportation Department (ITD) conducts bridge inspections in accordance with the National Bridge Inspection Standards (NBIS). ITD inspects 1,328 state owned bridges and 2,412 locally owned bridges on the National Bridge Inventory (NBI). The required inspection interval is 24 months. Some bridges of concern are inspected more frequently (12-month cycle) and if qualifying criteria is met, a few bridges are allowed to be increased to a 48-month cycle. Inspections are time-consuming and can pose safety risks to inspectors and the public if safety protocols are not followed. ITD uses under bridge inspection trucks (UBIT) to inspect 263 Idaho state bridges and 125 local bridges.

This report outlines a feasibility investigation into the use of Unmanned Aerial Systems (UASs) for use in bridge inspections, with the goal of identifying future uses and research. The research team conducted a literature survey on the applications of UASs in State Departments of Transportation (DOTs). Most state DOT research or internal investigations have used or studied UASs for surveillance and traffic control in the past, but recently, UAS-based bridge inspection has become a popular research topic. Current technology limits UAS use to an assistive tool for the inspector to perform bridge inspections faster, cheaper, and without traffic closure, in some situations. The major challenges for UASs include satisfying restrictive Federal Aviation Administration (FAA) regulations, position control in Global Positioning Systems (GPS) denied environments, pilot expenses, availability, and any required data post-processing.

The research team investigated two aspects of remote sensing in bridge inspections: visual inspection and autonomous defect detection, both using UAS inspection data. Several inspections on a lab made bridge using a 3DR Iris UAS showed UASs can be used for visual deck inspections and crack detection. An autonomous crack detection algorithm developed by the research team detected most of the deck cracks from the UAS inspection. In addition, the research team assessed the surface condition of two steel girders supporting the bridge deck during the inspection from a hand-held First-Person View (FPV) monitor. The research team investigated the construction of three-dimensional (3D) models of the entire lab-made bridge using UAS inspection images. The research team used an off-the-shelf program, AgiSoft PhotoScan, to create the model without extensive pre-processing on the inspection images, which could improve the model, but was also prohibitively time consuming. The model was unacceptable and incomplete, and the authors with ITD engineers decided that the entire process (pre-processing, model creation and post-processing) was too time-consuming to pursue for routine use.

The next phase of this study required the research team to determine the feasibility of fatigue crack detection using three UAS: 3DR Iris, DJI Mavic, and a custom-made octocopter called the Goose. The research team equipped each UAS with a visual camera. Then the research team identified the minimum requirements, in terms of camera distance to the defect of interest and lighting conditions, in which a test-piece with a known fatigue crack would be visible. In an indoor, GPS-denied, climate controlled space, the research team carried out a set of experiments to find the test-piece fatigue crack in the enclosed Utah State University structural lab. The crack was not visible in the images captured by the 3DR Iris due to its erratic flight control in absence of GPS signals and its camera specifications. The DJI Mavic pictures were acceptable since the UAS exhibited stable flight even without GPS and was able to navigate to within 20 to 25 cm (8 to 10 in.) of the defect and detect the fatigue crack even in low lighting

conditions. Similar to the 3DR Iris, the Goose relied mostly on GPS signals for control and failed to get close enough for fatigue crack detection. However, the Nikon camera, which was mounted on the Goose, had an optical zoom option which allowed the UAS to be 70 cm (30 in.) away from the area of interest.

The last step was to conduct inspections of an in-service bridge using UASs. This would allow the research team to evaluate the UASs' performance in GPS-denied and uncontrolled environments. The 3DR Iris had considerable difficulty maintaining control due to wind, and therefore the inspection images were unacceptable. The DJI Mavic could safely get close enough to the crack for real-time detection, and using the digital zoom in the camera helped acquire images with detectable fatigue cracks that could be seen on the cell phone sized viewscreen. The DJI Mavic camera has the ability to tilt the camera up to 30 degrees, which can limit visibility. The Goose was not flown under the bridge since the flight characteristics require more than the 2 m (6.5 ft) clearance between the bridge and ground to limit ground effects. The research team developed an image processing algorithm for autonomous fatigue crack detection, which identified more than 80 percent of the actual length of the crack in the DJI Mavic images. More images are required to evaluate the effectiveness of the algorithm. The research team recommends the DJI Mavic as a possible solution for under-bridge inspections due to its use of sonar signals in absence of GPS, camera quality with light exposure control, obstacle avoidance algorithms, and small size that allows it to maneuver in tight places.

In addition to visual images, the research team examined another non-contact method by performing passive (using only ambient heat) and active (using external heating sources) thermography experiments on the fatigue test-pieces from ITD. Two thermal cameras were used in the thermography experiments: a FLIR SC640 (with 1°C sensitivity) and a FLIR E8 (with 0.2°C sensitivity). The research team did not observe fatigue cracks in the thermal images taken in the passive case using the FLIR SC640. The E8 camera results were somewhat successful, but not useful for UAS inspection. It was shown that it is possible to use active thermography and the FLIR E8 camera for fatigue crack detection. Despite this success, thermography using UASs for fatigue crack detection is not feasible at this time because active thermography requires an external heat source.

Phase three of this study was to perform an inspection of a fracture critical bridge in Ashton, Idaho. The research team selected the DJI Mavic based on its performance in the previous tests. During the inspection, the minimum achievable clearance for UASs to avoid collision in gusty winds was 75 cm (30 in.). Only two of the previously detected fatigue cracks were inspected by this UAS since it was unstable over the river. The instability was because the UAS uses downward sonar signals for stabilization, which were confused by the fast-moving water. Fatigue cracks were not visible in the images. However, minor rusting and paint deterioration of the bridge girders, floor beams, girder splice, and other under-bridge members were visible using the inspection images. Concrete delamination, efflorescence, cracking in concrete, mild steel rust, and paint condition were detectable in the DJI Mavic pictures.

Chapter 1
Introduction

Research Motivation

The Idaho Department of Transportation (ITD) is responsible for inspection of 1,328 state bridges and 2,412 local bridges, listed in the National Bridge Inventory (NBI). ITD chooses to inspect the state bridges internally while using seven to ten consultant firms to conduct local bridge inspections periodically. ITD performs Inventory Inspections, Routine Inspections, Damage Inspections, In-depth Inspections, Fracture Critical Inspections, Special Inspections, and Complex Inspections. While emergencies do arise for which the Under Bridge Inspection Trucks (UBITs) may be needed (e.g. damage inspection), the UBIT is specifically programmed to be used for In-Depth Inspections, Fracture Critical Inspections, Special Inspections, and Complex Inspections, which cover 263 state bridges and 125 local bridges. With the exception complex bridges, the majority of the UBIT inspections are considered In-depth Inspections. According to the ITD bridge inspection manual section 4.2.3.3, an In-depth inspection is typically performed to: [1]

- Assess bridge elements not accessible during routine inspections.
- Obtain more sophisticated data.
- Perform special testing.
- Bring in other experts to assess particular problems.

The main reason for an In-depth inspection is to assess bridge elements. Bridge element assessments are the main motivation for researching Unmanned Aerial System (UAS) technology because inspecting with a UBIT adds additional expense and time to the inspection procedure, including but not limited to scheduling UBITs and maintenance of traffic. For this reason, ITD prefers to complete the inspection without a UBIT when possible. ITD has three full-time inspectors for the entire state covering 216,000 km^2 (84,000 mi^2) including 940 centerline km (612 centerline mi) of the Interstate Highway System. Two UBIT trucks and one full-time UBIT operator are accessible to ITD for all state and local bridge inspections. Inspections can involve exposure and other risks if safety protocols are not rigidly followed. Safety protocols often require additional personnel, training, and equipment. Thus, they can be costly but are necessary. A common routine bridge inspection requires one inspector to spend 20 minutes to 10 hours performing an inspection. Time required depends on the size and the complexity of the bridge. In addition to the time spent on the inspection, the inspector must provide a report to summarize their findings. Typically, writing a report takes up to 4 hours. Inspectors usually perform the inspection process using targeted visual techniques for more efficient and streamlined inspections. In targeted inspections, only regions with a high probability of a specified defect will be visually inspected.

Use of UASs for bridge inspection has the potential to improve this practice in Idaho by limiting the need for UBITs and decreasing inspection time in certain situations. This study is focused on evaluating the limitations of UAS capabilities in a targeted inspection, which is defined for the purposes of this report

as UAS inspection of a localized area for a specific defect, as opposed to observation of the entire bridge or several locations for any number of defects. One of several defects that ITD inspects for, and usually requires a UBIT, is steel cracking in the superstructure. Fatigue cracks are considered one of the most critical and hard to find defects for which UAS technology may be useful in aiding ITD inspectors. However, fatigue cracks are also the most challenging for UAS, specifically due to the environment, lack of GPS signals, variable pilot skill, and the typical locations of fatigue cracks. This report, while providing some preliminary qualitative inspections of some fabricated defects, is focused on determining if fatigue cracks can be detected on steel superstructures.

Use of UASs by ITD

ITD initiated a study in April 2014 to investigate the use of UASs in areas that could be dangerous or costly for a human inspector. In 2015, ITD district engineers authorized a Drone Pilot Project that would investigate the possibility of using UASs for ground surface gathering, bridge inspection, and construction inspection and documentation missions. The flight company selected was Empire Unmanned, with assistance from Advanced Aviation Solutions, which is now a subsidiary of Empire Unmanned. Three areas were selected for the Drone Pilot Project: the area around the I-15/US-30 interchange in Pocatello, Canyon Creek Bridge on SH-21, and the I-84 Snake River Bridges near Declo.

ITD project coordinators reported that the biggest barrier for these tasks was not technical, but regulatory. To fly commercially, the pilot operated under a Federal Aviation Administration (FAA) Section 333 exemption, which included a provision that all "non-participating personnel" could not be under the UAS for a 150 m (500 ft) radius. This meant that all traffic would have to be stopped while the UAS was in flight. Empire Unmanned secured clearance to fly over live traffic.

The first flight took place on May 18, 2015, on Interstate I-15 near the US-30 interchange in Pocatello, Idaho. The pilot flew the fixed-wing UAS, a Sensfly eBee RTk, twice, with a total flight time less than 30 minutes. The first flight was for traditional photogrammetry processing, where the ground targets would be used to place and scale the information taken by the camera. The second flight used a base station to send corrective information to the eBee so that the photos would have the correct information to make an accurate point cloud, eliminating the use of ground targets. This flight provided aerial photo mosaics and a point cloud of the area. The data for the pilot project is available from ITD's Research Program upon request.

The second flight was over Canyon Creek Bridge on SH-21, which is between Idaho City and Stanley. The plan was to use flaggers to stop traffic while a multi rotor UAS was used for the flights. Traffic control for the first flight had to be modified because flaggers had not arrived. A DJI Phantom UAS equipped with a visual sensor flew while observers on each side of the bridge watched for traffic. When a vehicle was spotted, the pilot would move the Phantom to a spot away from the roadway until the vehicle cleared the area, after which it would resume the flight. After the first flight, the flaggers arrived and a traditional flagger set up was used. The rest of the flights used a DJI S550 Flier, a six-rotor aircraft that held the thermal sensor. There were five total flights, with each flight lasting about 5 minutes. The deliverables included photo mosaics of both color and greyscale thermal imaging and a video of the

color thermal along with point cloud and surface data. However, the thermal images did not have high enough resolution to show any sign of delamination and were insufficient for bridge deck inspection.

The final areas were the I-84 Snake river bridges near Declo. That final flight took place June 22, 2015 and started with the placement of ground control points that would later be surveyed. The main flight was done with the eBee RTK and took about 20 minutes. After the eBee flight, a DJI Phantom surveyed the north side of the completed bridge from outside of the structure, enabling GPS-aided navigation. The research team extracted point clouds, surface photos, aerial photos, photos of the north side of the completed bridge, and a measurement of an on-site stock pile from the data. The next steps for the Drone Pilot project were to do follow up flights on SH-21 and I-84 and to continue processing the data that had been received so far. According to the ITD project leader, the results indicated that UAS inspections are a safe and effective way to gather data that can be used for design, construction, and ground monitoring purposes. According to district engineers, research projects will need to be done to test the accuracy and usability of the UAS data. Since the completion of this study, ITD Video has been used for UAS imaging of flooding during spring 2017 and documenting a historic bridge.

Research Objectives

The main research objective was to study the effectiveness of using UASs to detect steel fatigue cracks in a GPS-denied environment. Task 1 was to prove that UASs can fly safely in GPS-denied environments and to attempt to identify several defects on a lab made bridge. Task 2 was to perform a literature review and to determine limitations that exist when using UASs to perform an under-bridge inspection. Task 3 was to identify several UASs, cameras, lighting, and environmental conditions that UASs can detect fatigue cracks in, and to develop software that can automatically detect a fatigue crack from visual images. Task 4 was to perform an inspection of a recently inspected in-service bridge for fatigue cracks and compare the results to those of the inspection reports. Task 5 was to compile the final report.

FAA Regulations for Flying UASs

There are two sets of rules for flying any aircraft: Visual Flight Rules (VFR) and Instrument Flight Rules (IFR). According to the "Aeronautical Information Manual", a controlled airspace is defined as "…an airspace of defined dimensions within which air traffic control service is provided to both IFR and VFR flights in accordance with its classifications."[2] In the United States, the International Civil Aviation Organization (ICAO) designates controlled airspaces as stated in Table 1.

Table 1. Designated Airspaces in United States (Adapted from Aeronautical Information Manual [1])

Class	Definitions
Class A	From 5,500 m (18,000 ft) Mean Sea Level (MSL) up to and including Flight Level
Class B	From the surface to 3,000 m (10,000 ft) MSL; or around large airports
Class C	From the surface to 1,200 m (4,000 ft) above the airport elevation; or around midsize airport
Class D	From the surface to 760 m (2,500 ft) from the airport elevation or around small airports
Class E	A regulated airspace that is not classified as A, B, C, and D
Class G	Uncontrolled airspace with no IFR operation.

One of FAA's responsibilities is to provide safety regulations for flying UASs. FAA recognizes two categories for UAS use: "Fly for fun" and "Fly for work/business." The former does not require permission from FAA, but the vehicle should be registered through the FAA website. The "Fly for work/business" category is restricted by FAA. The latest version of the FAA rules was published on the FAA website on June 21, 2016.[3] Some of these regulations are as follows:

- The total weight of the unmanned aircraft should be less than 25 kg (55 lb).
- The vehicle must remain within the visual line-of-site of the remote pilot in command, the person manipulating the flight controls, and the visual observer during the flight.
- The aircraft must not operate over any persons that are not directly participating in the operation, are not placed under a covered structure, and are not inside of a covered stationary vehicle.
- Flight is only permitted during daylight or civil twilight with appropriate anti-collision lighting.
- The sole use of a first person view camera does not satisfy the "see-and-avoid" requirements.
- The maximum altitude is 133 m (435 ft) above the ground level, or within 133 m (435 ft) of a structure.
- The maximum speed of the UAS must not exceed 160 km/h (100 mph).
- No person may act as a remote pilot or visual observer for more than one UAS at the same time.
- The UAS operator must either hold a remote pilot airman certificate or be under the direct supervision of a certificate holder.
- UASs must be registered and certified by the FAA.
- The UAS must not be flown within 8 km (5 mi) of an airport without prior authorization from the airport operators.
- The UAS must not be flown from a moving vehicle.

Pilot requirements are:

- Must be at least 16-years old.
- Must pass an initial aeronautical knowledge test at an FAA-approved knowledge testing center.
- Must be vetted by the Transportation Safety Administration (TSA).
- Must pass recurrent aeronautical knowledge test every 24 months.

Based on these requirements, a certified pilot can fly a standard UAS under a bridge without traffic closure as long as the UAS is not flown directly over vehicles. However, it is possible to get a wavier for live traffic flights but it depends on the UAS altitude and location. If traffic is both above and under a given bridge, like in a flyover, the traffic under the bridge would need to be stopped to inspect under this bridge, just like the traffic would need to be stopped above the bridge to perform an inspection above the bridge.

Registered aircraft must have an application form (AC Form 5050-1) and evidence of UAS ownership. After submitting these documents, the UAS is registered and the pilot can request a Certificate of

Authorization (COA). The following information is required to submit the COA application form: concept of operation and type of the missions, operation location, altitude, communications, and flight procedures.[4] After submission, "… FAA conducts a comprehensive operational and technical review. If necessary, provisions or limitations may be imposed as part of the approval to ensure the UAS can operate safely with other airspace users. In most cases, FAA will provide a formal response within 60 days from the time a completed application is submitted…"[5] The COA application also requires proof of airworthiness for the UAS. This proof can be obtained either by submitting an Airworthiness Statement, or through FAA's Certificate of Airworthiness. Because of a new interim policy, FAA has been speeding up COAs, also known as certificate of waiver for section 333, for certain commercial UASs. Section 333 exemption holders now are automatically granted with "blanket 400-foot" which allows them to fly anywhere in the country except for restricted airspaces, as long as they are below 121 m (400 ft) and the UAS is not heavier than 25 kg (55 lb). The part 107 regulations provide a flexible framework, however, more opportunities have been provided by FAA to omit these regulations.[6] In order to illustrate the changes in recent rules Table 2 demonstrates the summary of the regulations for flying UASs and micro UASs (which weigh less than or equal to 2 kg [5.45 lb]) as of Otero et al. from 2015 [4] and now. It seems that restrictions have relaxed, the definition of UAS and micro UAS seems to have been removed, FPV is not allowed for the pilot and the operator certificate has been defied as the FAA Part 107 exemption. Operation near airports has been relaxed, with permission and operation of densely populated regions (densely is not rigorously defined by the FAA at this time) is only allowed with a waiver. Note that Autonomous operation is defined as any flight with a drone that the pilot-in-control is not in direct control of the UAS.

Table 2. UAS and Micro UAS Regulations (Adapted and Updated from Otero et al. [4])

Provision	From Otero et al. 2015[4]		As of this writing
	UAS	Micro UAS	UAS
Maximum Weight (UAS plus payload)	25 kg (55 lb)	2 kg (4.5 lb)	25 kg (55 lb)
Airspace confinements	Class G, and Class B, C, D, E with Air Traffic Center permission	Only Class G	Class G, and Class B, C, D, E with Air Traffic Center permission
Distance from people and structures	No operation over any person not involved and uncovered	No limitation	No operation over any person not involved and uncovered
Autonomous operations	Yes	No	Yes, but pilot in charge must be able to take control in emergency
First Person View (FPV)	Permitted; if visual line of sight is satisfied	Not permitted	Only by Visual Observer
Visual observer training	Not required	Not required	Not required
Operator training	Not required	Not required	FAA Part 107
Operator certificate	Required with knowledge test	Required without knowledge test	FAA Part 107
Preflight safety assessments	Required	Required	Required
Operation within 8 km of an airport	Prohibited	Prohibited	Prohibited without permission from Air Traffic Control
Operate in densely populated region	Permitted	Permitted	Prohibited without Waiver
Liability insurance	Not required	Not required	Not required
Night operation	Prohibited	Prohibited	Prohibited 30 minutes before and after civil Twilight

UAS Definitions

UASs are generally defined as any aircraft or aerial device which is able to fly without an onboard human pilot. They are also known as unmanned aerial vehicles, drones, remotely piloted aircraft, remotely operated aircrafts, remotely piloted vehicles, and remote controlled helicopters. Depending on the application, UASs are equipped with different types of non-contact sensors like visual cameras, thermal cameras, Light Detection and Ranging (LiDAR) sensors, ultrasonic sensors, etc. UASs' control and navigation are commonly carried out by Global Positioning Systems (GPS), Inertial Navigation Sensors

(INS), Micro-Electro-Mechanical Systems (MEMs), gyroscopes, accelerometers, sonar sensors, and Altitude Sensors (AS), all onboard a UAS.[7] The collection of the UAS platform, sensors, and control system form a system known as an Unmanned Aerial System (UAS).

GPS is a radio navigation system that allows land, sea, and airborne users to determine their location and velocity. INS is a navigation aid that uses a computer, a set of motion sensors, and a set of rotation sensors to continuously calculate the position, orientation, and velocity (direction and speed of movement) of a moving object without the need for external references. It is used on vehicles like ships, aircrafts, submarines, guided missiles, and spacecraft. MEM is the technology of microscopic devices, particularly those with moving parts.

An Unmanned Aerial System (UAS) consists of three parts, according to the Association for Unmanned Vehicle Systems International (AUVSI): the vehicle that might be an aircraft, a multi-copter, or a helicopter; payload that includes the weight of all sensors mounted on the vehicle; and the ground control system or station, which sends commands to the vehicle for takeoff, positioning, and landing. Based on size, weight, endurance, and range of flying altitude, there are three classes of UASs: tactical, strategical, and special task.[7] The UASs usually used in civilian applications, such as bridge inspection, are classified as tactical UASs, as defined in Table 2. However, the designation between microUAS and UAS seems to be arbitrarily defined by different sources and is not an FAA designation[4, 8].

Interpretation of Photographic Images

In this study, several images, visual and thermal, of bridge structures, real or simulated, were evaluated. In all cases images were evaluated by the same inspector. This inspector had a Master's degree in structural engineering, but no bridge inspection training. Images were viewed on different media, cell phone and desktop screens, as noted in the sections below.

Pilot

Only a single pilot was used from the start to the end of this study for the presented investigations. This pilot obtained his part 107 FAA UAS license at the beginning of the study and was therefore relative novice at flying UASs, by the end of the project he had logged 110 hours on this and other endeavors.

Archived Data

All experimental data presented, organized by experiment number, is available from ITD's Research Program upon request.

Chapter 2
Literature Review

UAS Applications for Bridge Inspection

Several states have investigated UAS applications for numerous state DOT missions such as traffic surveillance, avalanche control, mapping, construction project monitoring, bridge inspection, etc. In this section, studies conducted on using UASs for bridge inspections are briefly presented.

California

In 2008, California DOT and University of California at Davis published a report on bridge inspection using aerial robots.[9] The researchers designed a custom UAS to be tethered to the ground, therefore making it easier to control and conform to the FAA regulations at the time. The researchers then mounted a high-resolution video camera on the UAS with forty-five-degree tilt. Next, the researchers developed the onboard Flight Control Computer to provide a redundant high-speed communications link to manage the UAS stability. California DOT terminated the project because it did not result in a fully-deployable aerial vehicle due to the following problems: unreliable heading sensor data (heading sensor is an earth's magnetic field sensor which was used as a compass), instability (especially in wind), and unsuccessful implementation of an altitude holder sensor. The California research project was one of the first known research projects done by DOTs for utilizing UASs in bridge inspections.

Georgia

In 2014, Georgia Institute of Technology and Georgia DOT published the outcomes of 24 interviews with Georgia DOT personnel. The goal of these interviews were to evaluate the economic and operational advantages and drawbacks of UASs within traffic management, transportation, and construction.[10] The Georgia study included an investigation of five different UAS configurations, A through E. System A was a quad-motor UAS with FPV, Vertical Take-off and Landing (VTOL), and a video camera suitable for monitoring operations such as, but not limited to, traffic monitoring. System B was an enhanced version of System A, equipped with LiDAR. Georgia DOT recommended this system for any mission that involved mapping. System C expanded upon System A, with emphasis on prolonged environment/region monitoring in areas such as construction sites. System D was proposed as a UAS for county-sized missions, whereas Systems A through C were regional. A fixed-wing aircraft with a wingspan size of 2 m to 6 m (6.5 ft to 20 ft) and capable of high-quality aerial photogrammetry comprised System D. This system was suggested as a proper candidate for post-disaster response missions and highway control. Finally, System E configuration, which was recommended for bridge inspections, consisted of a multi-rotor copter with eight or more motors, potentially tethered, capable of VTOL, and equipped with LiDAR and safety pilot mode.

Michigan

Michigan DOT published the results of their experiments on five UASs.[11] These UASs were equipped with a combination of visual, thermal, and LiDAR sensors to assess critical infrastructure and their issues, for example bridges, confined spaces, traffic flow, and roadway assets. Researchers concluded that UASs are a low-cost, flexible, and time-efficient tool that can be used for multiple purposes: traffic control, infrastructure inspections, and 3D modeling of bridges and terrain. Michigan DOT reported each UAS to be suitable for a specific task in Michigan DOT. A VTOL UAS, equipped with thermal and visual cameras, proved to be the most appropriate for high-resolution imaging of a bridge deck. A VTOL UAS was able to calculate the locations and volumes of the spalls and delaminations of bridge decks. The deck inspection using non-contact sensors had mixed results when compared to hammer sounding results. These issues stemmed from the many patches and materials used to repair concrete, spalls, and other surface discontinuities present on bridge decks (i.e. there was no surface homogeneity).

Minnesota

Minnesota DOT initiated a comprehensive investigation of the benefits and challenges of UAS bridge inspection[12]. Collins Engineering inspected four bridges in Minnesota using UASs to study the effectiveness of VTOL UASs. The first bridge inspection was a 26 m (85 ft) long single span prestressed concrete bridge. The UAS could not perform an under bridge inspection due to low-clearance and lack of GPS signal. The human inspection and the UAS inspection detected bridge deck and rail defects like spalls and cracking. The inspector detected missing anchor bolt nuts during the under-bridge inspection, while the UAS was unable to detect this defect. However, mild scour was only detected by UAS images. A stitched model of the bridge deck was generated after the deck inspection. The second bridge inspection was a 100 m (330 ft) long open spandrel concrete arch bridge. The UAS could not survey the bridge deck due to traffic. The UAS also could not maneuver under the bridge due to the absence of GPS signals, but a zoom lens provided reasonable visibility for some under-bridge items. In this case, the reported mild scour was not detectable in the UAS images. This time the UAS inspection results showed bearing deterioration, which the previous human inspection missed. On the third structure, a five-span steel underdeck truss was inspected by UAS. The UAS investigated the truss superstructure and substructure and the results were in close agreement to the human inspection results. The final bridge was approximately 850 m (2,800 ft) with five truss arch spans. The UAS inspection was carried out, but it was not compared to a human inspection. Collins Engineering concluded that UASs can be used for bridge inspection while posing minimum risk to the public and the flight personnel. In some cases, UAS images provided a cost-effective way to obtain detailed information that may not normally be obtained during routine inspections. FAA regulations prevented the team from flying UASs over traffic, negating the benefits of UAS inspections for the deck.

Florida

Florida DOT (FDOT) began to investigate the applications of UASs in 2005 with the main focus on traffic management and road monitoring.[13] In 2015, FDOT published another UAS research project investigating the feasibility of UAS bridge inspection and high mast luminaires.[4] A UAS, equipped with high-definition cameras, was used in lieu of experienced inspectors to achieve the following goals: reduce the cost of inspection, reduce the hazards to the inspector, increase the public safety, and increase the inspection effectiveness through more comprehensive data acquisition. Limitations were also identified: allowable payloads, control and navigation in severe winds, and poor image quality in low-light conditions.

One of the goals of this study was to select the main UAS components based on the demands of the project. The researchers developed a weighted factor analyses to provide a systematic decision-making toolbox for each component. This led the research team to select three VTOL UASs, four ground viewing stations, and three visual cameras. Finally, the researchers selected a dual camera setup and a remote control gimbal on a six rotor UAS to perform the inspections. This UAS was tested for flight in windy conditions. The UAS's closest distance from an object was estimated at 0.3 m (1 ft) for wind speed less than 11 km/h (7 mph) and wind gusts less than 16 km/h (10 mph). In addition, the final report recommended 1 m (3 ft) clearance in wind speeds greater than 24 km/h (15 mph) and wind gusts greater than 32 km/h (20 mph). FDOT found that UASs can collect inspection data for a high mast luminaire in 8.5 minutes while providing adequate pictures in acceptable detail.

Additionally, the research team performed two preliminary field tests at the Florida Institute of Technology campus under controlled conditions; a pedestrian bridge and a wooden bridge were inspected under 15 minutes. The inspections indicated moderate and severe rust on welded or bolted structures, a longitudinal crack along the guard rail, and a small stress crack on the beam underneath.

The research team also participated in a field test with FDOT inspectors and performed the inspection in 10 minutes while subject to 20km/h (12 mph) wind speeds and 29 km/h (18 mph) gusts. Rust, cracks through epoxy, bearing deformation, and deck and girder separation were among the detected flaws. The other field test was performed on a steel railroad drawbridge with the wind speed at 11 km/h (7 mph) and the wind gusts at 27 km/h (17 mph). The team detected missing nuts and severely rusted bolts. The team performed the third field inspection on a concrete and steel superstructure bridge in 10 minutes with the wind speed at 27 km/h (17 mph) and the wind gusts at 40 km/h (25mph). This inspection showed mild to severe corrosion regions on transverse girder bracing and separation between the girder and the deck in the images. One new aspect the FDOT research introduced was a service and maintenance schedule for UASs. The research team recommended inspecting motors, propellers, airframe structure, and batteries at least every 25-hours of operation.

Literature Review Summary

This chapter presents the past applications of UASs in DOTs. Figure 1 shows states with either past or current investigation of UASs in red. Although most of these research projects have not been focused on bridge inspections, UASs have been a fast-growing technology in the area of bridge inspection for the past a few years. Table 3 summarizes the conducted DOT funded UAS related research for bridge and infrastructure inspections. Table 4 summarizes the inspection tasks attempted by the different studies focused on bridge inspection.
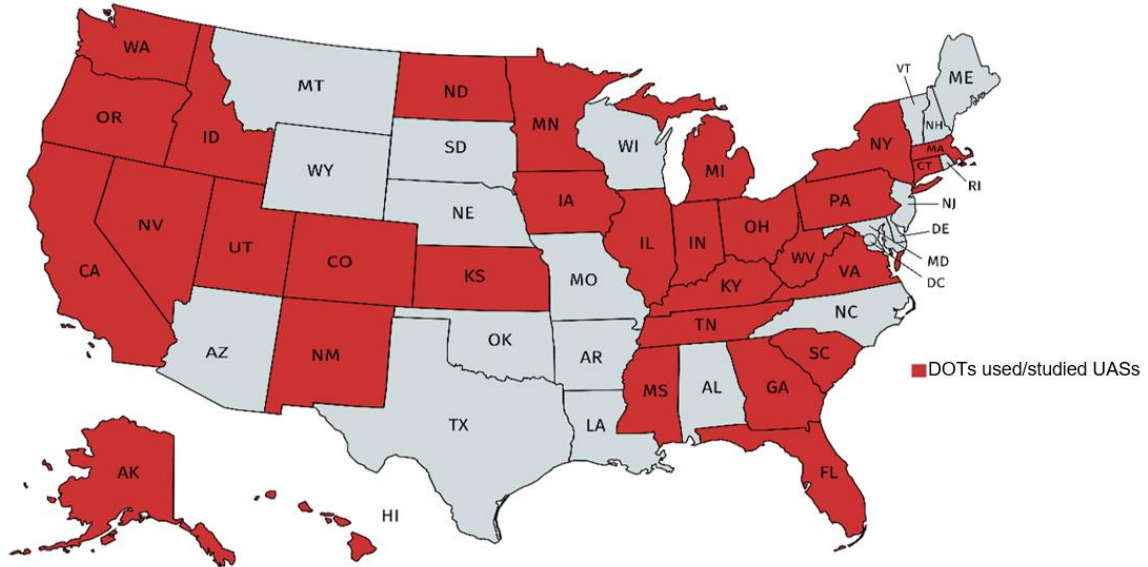
Figure 1. Map of State DOTs that Have Documented Past or Current Study of UASs

Table 3. Civil Infrastructure Condition Assessments Using UASs

State DOT	Year	UAS	Inspection Achievements	Inspection Challenges
California	2008	ES20-10	Inspection was not performed	UAS Instability and control issues
Georgia	2014	N/A	Proposition of five UAS	Actuall inspections were not performed
Michigan	2015	Bergen HexaCopter, DJI Phantom, BlackoutMini Quadcopter, Heli-Max 1 Si.	Autonomous spall detection Deck 3D model reconstruction Deck delamination detection using thermal images Thermal and visual combination Successful pump station and culvert inspections using drones	The automated spall detctor understimated the actuall spall area Thermal inspections were inaccurate because of the variation in surface emissivity of the deck Non-automated navigation and controlling system Inaccurate GPS
Minnesota	2015	Aeron Skyranger	Defect detction: cracks, spall, scour, missing bolts, Building the map of the structure, IR technology to detect delamination, Reasonable agreement between the results of UAS and visual inspections	FAA regulations prevented deck inspection Loss of GPS signals
Florida	2015	ArduPilot Mega 2.5 Micro Copter	Defect detection: cracks, spall, scour, missing bolts Reducing inspection cost and time in high mast luminars	FAA regulations prevented deck inspection, No under-bridge inspections, Control issues in wind speed greater than 25km/h, Low quality images in severe weather condition

Table 4. Summary of Attempted UAS Bridge Inspection Tasks

State DOT	Year	Under-bridge UAS inspection	Steel crack detection	Concrete Surface Defection Detection	Concrete Delamination Detection	Visual Camera	IR Camera
California	2008	N	N	N	N	Y	N
Georgia	2014	N	N	N	N	N	N
Michigan	2015	N	N	Y	Y	Y	Y
Minnesota	2015	N	N	Y	N	Y	N
Florida	2015	N	N	Y	N	Y	N

Chapter 3
Small Bridge Experiment

The goal of the small bridge experiment was to simulate UAS bridge inspection on a lab-made bridge with predefined defects to determine the performance, shortcomings, and demands for UAS bridge inspection. For this purpose, a small bridge measuring 6 m (20 ft) long, 4 m (13 ft) wide, and 0.2 m (8 in.) thick (deck thickness) was built at the Systems, Materials, and Structural Health (SMASH) lab of Utah State University. The small bridge is shown in Figure 2. The research team made the bridge from on-hand materials used in previous research projects. The pre-existing defects on this structure were concrete cracks, lightly corroded girders, and deck delamination. Concrete cracks were located on the top and bottom of the concrete deck. The bridge deck was supported by two steel girders. The girders had mild surface corrosion along the webs, the flanges, and the web stiffeners. The research team implanted the deck with subsurface delamination, formed by thin sheets of plastic, at the time of construction.

Figure 2. Small Bridge at the SMASH Lab

At this point in the study, only a 3DR Iris UAS equipped with a GoPro Hero 4 camera was available. A schedule of the experimental damaged specimens is presented in Table 5. A schedule of experiments performed on the small bridge is presented in Table 6 and outlined in more detail below. Appendix A of this report provides a complete list of the specimens and experiments carried out in this study.

Table 5. Schedule of Specimens for Small Bridge Experiment

Specimen ID	Source	Defect	Form	Dimensions	Location
S01	USU	Surface Concrete Cracks	Lab-made Bridge deck	20' x 13' x 0.75'	SMASH Lab
S02	USU	Surface Corrosion	Steel Girder 1	W10 x 88	SMASH Lab
S03	USU	Deck Delamination	Lab-made Bridge deck	20' x 13' x 0.75'	SMASH Lab

Table 6. Schedule of Experiments for Chapter 3

Experiment ID	Intent	Specimen	UAS	Camera	Site	Page on The Report
E001	Detect Concrete Cracks (Manually)	S01	3DR Iris	GoPro Hero 4	SMASH Lab	16-17
E002	Detect Concrete Cracks (Autonomously)	S01	3DR Iris	GoPro Hero 4	SMASH Lab	17-18
E003	Detect Concrete Delamination	S03	3DR Iris	FLIR E8 Thermal Camera	SMASH Lab	19-20
E004	Detect Steel And Weld Corrosion	S02	3DR Iris	GoPro Hero 4	SMASH Lab	20-21
E005	3D Model Construction	S01	3DR Iris	GoPro Hero 4	SMASH Lab	21-22

Concrete Surface Cracks

The cracks on top of the bridge deck were detectable in real-time using the FPV monitor, E001, as seen in Figure 3. The shortest crack was approximately 2 cm (1 in.) long, whereas the longest cracks on the deck were roughly measured up to 50 cm (20 in.). The UAS was flown within about a 1 m (3 ft) clearance of the deck. The majority of the cracks were visible in real-time. Figure 4 shows an image from the inspection video where arrows indicate the detectable cracks and barely detectable cracks in the inspection image.

Figure 3. Example of Top Cracks in the Color Image Acquired by the UAS, E001
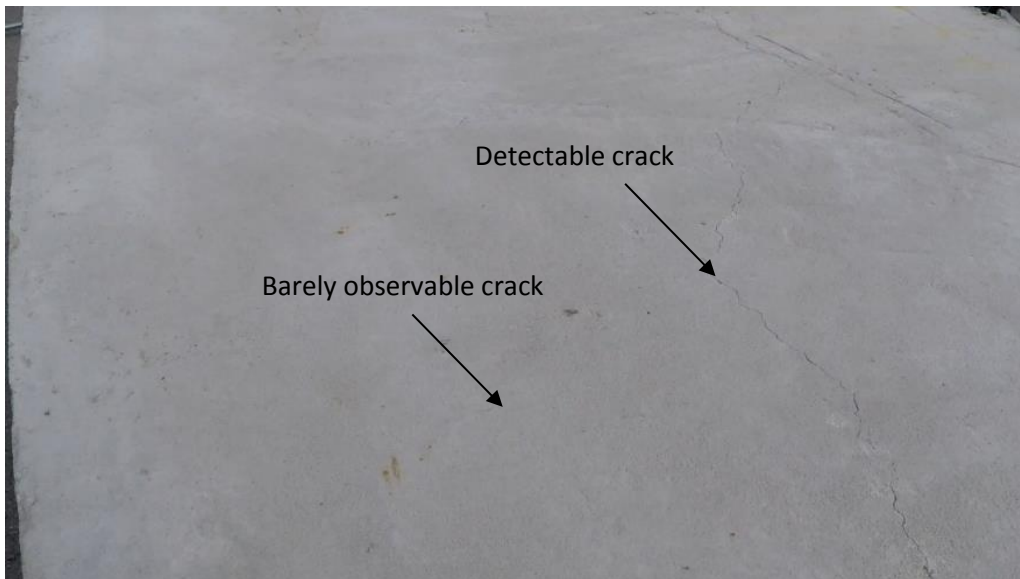
Figure 4. Variety of cracks' Dimensions on the Bridge Deck, E001

Automated Concrete Surface Crack Detection

Monitoring and measuring cracks are common practices in bridge deck and road pavement inspections. One-hundred and six color images were used as a dataset to evaluate a crack detection algorithm that the research team developed (E002).

For the purposes of this report, the standard image processing definition of accuracy (termed detection in this report) is defined as a weighted average of True Positive and True Negative reports. True positive is defined when a crack is detected by the algorithm while True Negative occurs when the algorithm finds no cracks in a sound image. In this report, when the algorithm finds more than 50 percent of the length of the crack in the defected dataset (determined visually by the research team), it is considered a True Positive. True Negative is considered when the algorithm finds no connected components resembling cracks in the sound dataset or when it provides a clutter-free image. This definition allows comparison to other crack detection algorithms in the image processing literature.[15] The crack detection algorithm used in this report had a 90 percent detection rate. Both of these results were more accurate than other contemporary visual image crack detection algorithms, one of which, when coded and used to analyze this same dataset, could only detect 45 percent of the cracks on this dataset[16, 17]. Other crack detection algorithms in the literature report similar or lower numbers than the algorithm developed in this report (for example: 64 percent to 86 percent [18], 73 percent[19] 90 percent[20]), although these are detected on different datasets. The Matlab code for the proposed concrete crack detection method is provided in Appendix B. The number of successful detections can be further increased by using better cameras, closer distance to the surface, more stable UAS, etc. Figure 5 shows the intermediate results of the crack detection algorithm on one of the images from the dataset.
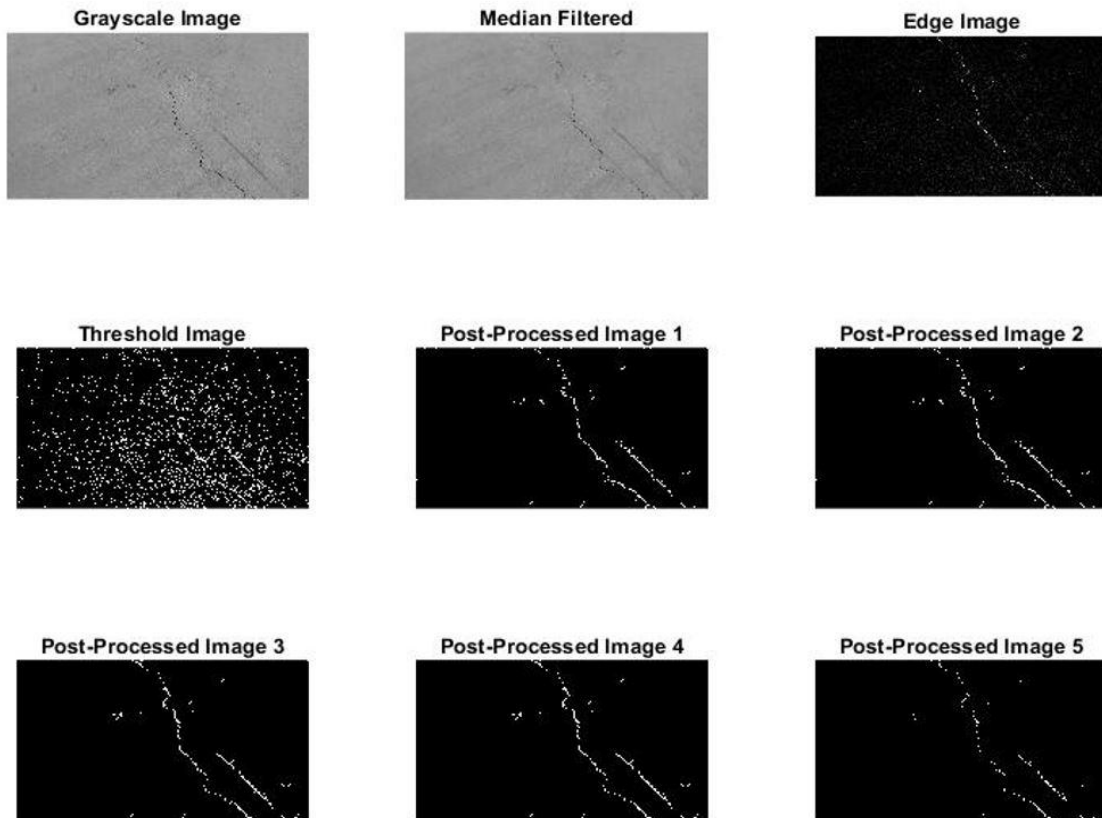
Figure 5. Automatic Crack Detection Based on UAS Images, E002

Deck Thermal Inspection

The research team also used the deck to investigate thermal delamination detection using an FLIR E8 thermal camera, E003. For this experiment, the FLIR E8 was mounted on the 3DR Iris, which maxed out the payload, making it only able to fly a short distance off the ground for a short period of time, which is why the slab was not mounted on the girders of the small bridge. A smaller thermal camera was not available. Even with this limitation, this experiment shows that it is possible with additional time and effort to detect subsurface (delaminations) and surface (cracks). A 0.6 m (2 ft) by 0.9 m (3 ft) plastic sheet inclusion was embedded in the deck during construction to simulate a delaminated region (see Figure 6). The research team monitored the bridge deck when the deck was still hot from the day and ambient temperature was dropping (deck temperature was roughly 25°C (70°F) on average. The thermal image is shown in Figure 7. The delaminated region was detectable as a cold region in the thermal image. However, there are other cold regions not associated with the depicted delamination in Figure 6, which had severe cracking in those areas that could also be identified visually. These cracks effectively altered the surface, which caused faster heat loss than the surrounding sound concrete, and they presented comparatively colder spots. This small experiment proved that using thermal imagery for surface and subsurface defect detection is feasible, however, it was not the focus moving forward.
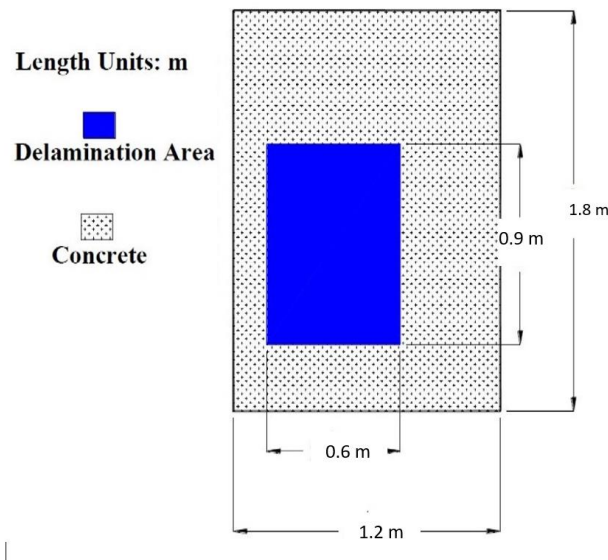
Figure 6. The Plan and Elevation View of the Deck and its Delamination, (E003)
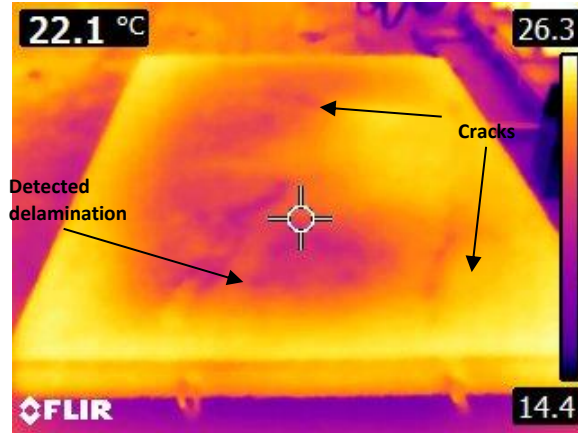
Figure 7. Captured Thermal Image, E003

Girder Inspection

The steel girders of the small bridge had minor surface corrosion which was visible in the real-time inspection videos (E004, see Figure 8). The distance between the UAS and the girder in Figure 8 was about 1 m (3 ft), similar to that recommended by Otero et al. in moderate wind conditions.[4] In addition to corrosion on the girders, the weld quality of the web stiffeners was observable in real-time using the optical zoom feature (Figure 9). The camera the research team used for this inspection was a GoPro Hero 4, which is not ideal for scientific and accurate imagery due to its focal length and fish eye effect (see rounded edges of objects in corners of Figure 8). However, GoPro cameras are very popular for UASs due to their small size and light weight. Better cameras are likely to produce better results.

Figure 8. Steel Girder Surface Corrosion and Rust in the Image Acquired by UAS, E004

Figure 9. Visual Weld Inspection on the Small Bridge, E004

Off-the-Shelf 3D Model Reconstruction

The research team imported eight-hundred and forty images of the bridge to Agisoft PhotoScan, a commercial 3D model reconstruction software, to generate 3D models from 2D images (see Figure 10), E005. [21] No modifications or pre-processing operations were applied on the images before the model was constructed. The total processing time took about 16 hours. This execution time could be reduced considerably if the preliminary modification and masking operations were carried out before the 3D model generation. Regardless, ITD engineers considered this to be too much time, especially because many parts of the bridge were missing or partially missing. Additional effort could improve this model, but the time investment was not thought worth it by ITD engineers.

Figure 10. Agisoft PhotoScan 3D Model of Small Bridge, E005

Lessons Learned from the Small Bridge Experiment

Based on the small bridge experiments (E001-E005), the following observations can be made:

- Image processing techniques (3D mapping or damage detection) that can detect defects are a significant advantage of UAS inspections, but must be tailored to the situation. Also, 3D mapping is not likely to be useful without significant effort and algorithm improvement.
- Real-time and autonomous concrete deck crack detection is possible using UAS based images.
- The light girder corrosion was detectable in real-time.
- Concrete delamination detection was shown to be feasible using thermography and is a promising area of additional research.
- Image processing techniques can be used to facilitate concrete crack detection and show promise for automated detection in real-time.

Chapter 4
Fatigue Crack Detection Requirements

Finding fatigue cracks is a difficult and expensive task in bridge inspection. These cracks often occur in under-bridge members and can be troublesome for the bridge inspectors to access. This chapter investigates the potential of UASs equipped with visual cameras to detect fatigue cracks (E006, E007, and E008). First, the research team determined the required conditions for fatigue crack detection through controlled indoor experiments. These experiments were performed on a test-piece with an existing fatigue crack which was provided by ITD. The purpose of this test was to determine the optimum camera distance and lighting conditions for three different cameras designated to three different UASs. The UAS were then used to inspect a test-piece, which contained a fatigue crack, in a controlled environment (E009, E010, and E011) and in an uncontrolled environment (E012 and E013). The SMASH lab was selected as the controlled environment and an in-service bridge owned by the Utah Water Research Laboratory (UWRL) was selected as the uncontrolled environment. This was done in order to assess the limitations of UAS-based fatigue crack detection. The visibility of the fatigue crack in the captured images was assessed for each UAS under different circumstances. The research team developed an automated crack detection algorithm to detect the fatigue cracks in the captured images autonomously. The feasibility of using active and passive thermography to find the fatigue cracks on two test-pieces acquired from ITD have also been investigated. This chapter represents the summary of findings and provides some guidance for visual and thermal image based fatigue crack detection using UASs.

Fatigue Definition

Fatigue is the tendency of a member to fail at a stress level below the elastic limit when subjected to cyclical loading. Fatigue cracks often are formed in load-bearing steel members during cyclic service loads and can result in the brittle fracture of the member. A fracture critical member (FCM) is a steel member in tension, or with a tension region, whose failure would probably cause a portion of the entire bridge to collapse. If the bridge system is "fracture critical" it requires a fracture critical member inspection, which consists of a hands-on inspection of FCM's or FCM components that may include visual and other non-destructive evaluation.

There are three stages to crack growth: Stage 1: Initialization stage, when the crack starts at an internal flaw or change in geometry; Stage 2: Propagation Stage, growth of the crack (the stage in which there is the opportunity to find the crack and arrest or repair it); and Stage 3: Fracture Stage, failure occurs when the member breaks into pieces. Fracture is the local separation of material into two or more pieces when subject to stress. Fracture is initiated from a flaw in either material or design and when it reaches a critical size it may cause the member to rupture. Fatigue cracking normally occurs slowly with somewhat slow crack propagation, whereas fracture occurs abruptly without warning. [22]

Current Practice for Fatigue Crack Detection

Finding fatigue cracks has been a major challenge in bridge inspections, mostly because fatigue cracks are short in length and very narrow in width. Fatigue cracks usually occur in under-bridge members and connections that are difficult to access by conventional physical procedures. Also, the steel members and connections are usually covered with rust and other surface clutter, which makes visual detection difficult if not impossible. In addition, the low-light conditions under bridges are another challenge in visual fatigue crack detection. The current process for fatigue inspections includes a visual or physical inspection (i.e. rust removal) and application of a suitable nondestructive evaluation (NDE) method such as dye penetration or magnetic particles, if necessary, to locate the cracks. [23] Finding the cracks in this manner can be expensive, dangerous, and time consuming.[24]

Image-based flaw detection methods have gained considerable popularity in the past decade. However, with regard to bridges, most of the effort has been focused on two types of defects: surface concrete cracks and subsurface concrete delaminations using infrared thermography.[24, 26] Finding fatigue cracks is especially challenging when using visual images. For instance, the size, shape, and intensity gradient of surrounding pixels of a fatigue crack are different from conventional concrete cracks. Thus, the previously developed algorithms are not appropriate to detect them. In addition, the efficiency of these algorithms is tied to the quality of the image, which could be a function of camera specifications, lighting condition, camera distance, etc.

Selected UASs

The research team used three UAS to perform bridge inspections and defect detections in this Chapter and are listed in Table 7.

Table 7. Investigated UAS for Fatigue Crack Detection

UAS	3DR Iris	DJI Mavic	Goose
Cost	<$500	$1,000	$ 5,000
Weight	1,282 g (2.8 lb)	743 g (1.62 lb)	11,400 g (25.2 lb)
Type	Quadcopter	Quadcopter	Coaxial Octocopter
Flight Time	16-22 minutes	27 minutes	27.5 minutes
Payload	400 g (0.8 lb)	900 g (2 lb)	14,400 g (32 lb)
FPV Broadcasting	yes	yes	no
Camera	GoPro Hero 4	DJI camera	Nikon
Obstacle Avoidance	no	yes	no
GPS-denied Altitude Measurement	no	Sonar	Barometer

Fatigue Crack Detection-Minimum Conditions

This section reports the results of a set of indoor experiments, E006 through E008. These experiments were performed to determine the requirements for three types of cameras performing fatigue crack detection. The requirements are in terms of lighting conditions and camera distance. For these experiments, a single test-piece with a known fatigue crack was observed under different conditions

(UAS, camera, lighting, and environment). For the beginning of this section, only a single fatigue test-piece was available and a second was obtained near the end of the project, as seen in Table 8. Only additional thermographic experiments were run on the second test piece. Table 9 summarizes the list of experiments performed in this chapter, much of which is detailed in the coming sections.

Equipment

Three cameras were used in these experiments:

- GoPro Hero 4, up to 12 Mega-Pixel (MP) with 4000 by 3000 resolution, which is compatible with the 3DR Iris and many others.
- DJI camera, 12 MP with 4000 by 3000 resolution, which was the onboard camera of the DJI Mavic.
- Nikon COOLPIX L830, 16 MP, 4068 by 3456 resolution, which was selected to be mounted on the Goose.

Table 8. Steel Test-Piece Schedule

Specimen ID	Source	Defect	Form	Dimensions	Origin
S04	ITD	Fatigue Crack	Steel Puck 1	D= 1.65" (4.2 cm)	Unknown ITD Bridge
S05	ITD	Fatigue Crack	Steel Puck 2	D = 1.65" (4.2 cm)	Unknown ITD Bridge

Table 9. Schedule of Experiments in Chapter 4

Experiment ID	Intent	Specimen	UAS	Camera	Site	Page in the report
E006	Detect Fatigue Crack (Minimum Requirements)	S04	N/A	GoPro Hero 4	Indoors (Office)	27-28
E007	Detect Fatigue Crack (Minimum Requirements)	S04	N/A	DJI Built-In	Indoors (Office)	30, 33
E008	Detect Fatigue Crack (Minimum Requirements)	S04	N/A	Nikon Camera	Indoors (Office)	30, 34
E009	Detect Fatigue Crack (Simulated Visual Inspection)	S04	3DR Iris	GoPro Hero 4	Indoors (SMASH Lab)	35, 37
E010	Detect Fatigue Crack (Simulated Visual Inspection)	S04	DJI Mavic	DJI Built-In	Indoors (SMASH Lab)	35, 38, 39
E011	Detect Fatigue Crack (Simulated Visual Inspection)	S04	Goose	Nikon Camera	Indoors (SMASH Lab)	35, 40
E012	Detect Fatigue Crack (Simulated Visual Inspection)	S04	3DR Iris	GoPro Hero 4	Outdoors (UWRL)	42-45
E013	Detect Fatigue Crack (Simulated Visual Inspection)	S04	DJI Mavic	DJI Built-In	Outdoors (UWRL)	44, 46-49
E014	Detect Fatigue Crack (Autonomously)	S04	DJI Mavic	DJI Built-In	Outdoors (UWRL)	51-53
E015	Detect Fatigue Crack (Passive Thermography)	S04	N/A	FLIR SC 640	Indoors (Office)	54-55
E016	Detect Fatigue Crack (Passive Thermography)	S05	N/A	FLIR SC 640	Indoors (Office)	54, 56
E017	Detect Fatigue Crack (Passive Thermography)	S04	N/A	FLIR E8	Indoors (Office)	56-57
E018	Detect Fatigue Crack (Passive Thermography)	S05	N/A	FLIR E8	Indoors (Office)	57-58
E019	Detect Fatigue Crack (Active Thermography)	S04	N/A	FLIR E8	Indoors (Office)	58, 60
E020	Detect Fatigue Crack (Active Thermography)	S05	N/A	FLIR E8	Indoors (Office)	50, 61, 62

Lighting Condition Definitions and Camera Distance

Lighting conditions play a major role in any sort of photogrammetry. The research team considered three lighting conditions to simulate different scenarios during the bridge inspection:

- "Dark", which is the approximation of the lighting conditions under a bridge during the daytime (according to USU onsite bridge), illumination range: 20-100 lx.
- "Normal", which is equivalent to the lighting conditions of a room with lights on, illumination range: 100-250 lx.
- "Bright", which is equivalent to the lighting conditions of a concentrated light source such as a flashlight, with illumination more than 250 lx.

Illumination was measured using a cell phone light meter app, "Light Meter" installed on an iPhone 6. While, not the most accurate luminance measuring device, off 35% from a light meter, on average, it was shown to provide acceptable relative measurement within the range of lux conditions in this investigation. [26] In addition to the lighting conditions, the distance between the camera and the object of interest affects the images. To determine the performance of each camera, the indoor experiments were also performed from different camera distances: 5 cm (2 in.), 10 cm (4 in.), 15 cm (6 in.), 20 cm (8 in.), 25 cm (10 in.), and 30 cm (12 in.). The 30 cm (12 in.) case is the most realistic scenario without using a zoom feature and the remaining were incremented down in 5 cm increments from the most realistic case.

Indoor Office Procedure

The research team placed the test-piece indoors under variable lighting conditions. Lighting conditions were varied by measuring the test-piece surface illumination. The cameras were set in front of the test-piece and a picture was taken for each camera distance and lighting condition.

Indoor Office Results

After the research team carried out the indoor experiments, the images were viewed on a conventional desktop computer to determine the requirements for locating the crack without any image enhancement features. The maximum distance for each camera in each lighting condition was reported as the required camera distance if the crack was detectable visually.

GoPro

The GoPro camera provided reasonable video quality in past tests for general inspection purposes and is very popular for UASs due to its small size and light weight. This camera performed poorly in the Dark condition from all proximities and the crack was not visible in any taken images, see Figure 11(a). The surface of the test-piece was blurry at the 5 cm (2 in.) camera distance, as seen in Figure 11(b), and the crack was not detectable, E006. However, the crack can be seen in the images with 10 cm (4 in.) and 15 cm (6 in.) camera distances. The GoPro cameras use the ultra-wide angle lens to provide larger length of field and a better aperture setting, but using these lenses causes severe distortion (known as the fisheye effect) in the captured images. The ultra-wide angle lens used in the GoPro camera is also a fix-focus lens with a short focal length. That is why the close-up images taken by this camera from the test-piece were oftentimes worse than the images taken with greater camera distance.

The maximum camera distance for the GoPro camera in the Normal condition was 20 cm (8 in.), which is shown in Figure 12. The GoPro pictures, taken in the Bright condition, were not satisfactory because light reflections in the pictures washed out the crack. Even though the GoPro camera captured the fatigue crack at 20 cm (8 in.) in the Normal lighting condition, it is not recommended to use the GoPro Hero 4 camera for fatigue crack inspection.

(a)   (b)
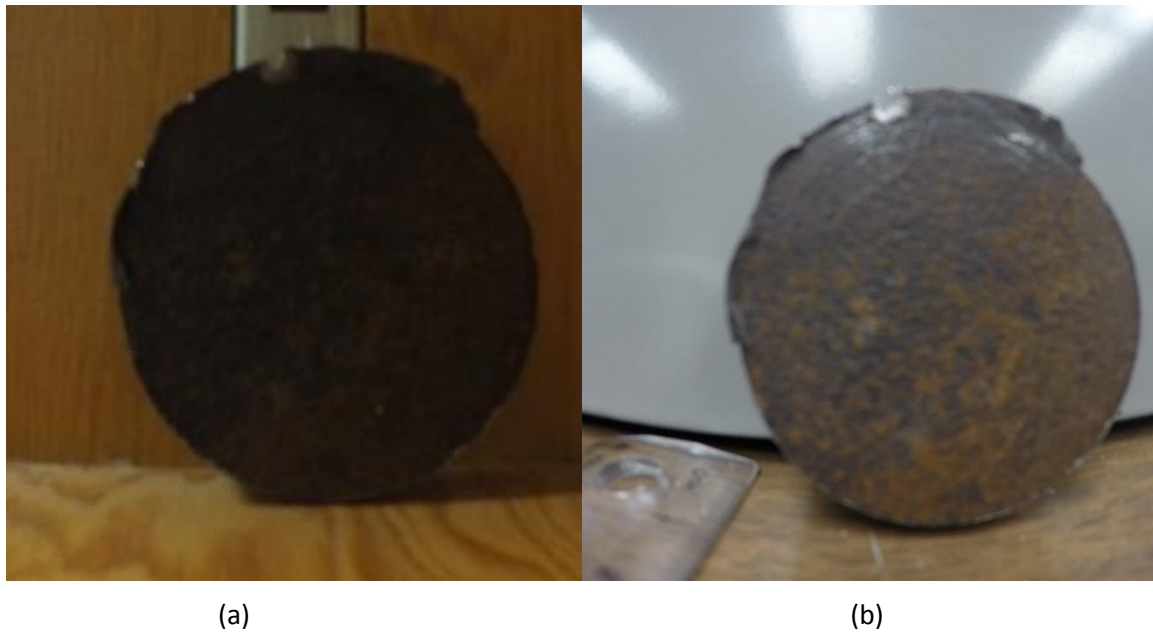
Figure 11. (a) Dark Condition, 10 cm (4 inches), GoPro (b) Normal Condition, 5 cm (2 inches), GoPro, E006

DJI Camera

The DJI Mavic has an onboard camera which was used to take the pictures, E007. The crack was not visible in the images taken in the Dark condition without exposure adjustment, however, the DJI Mavic camera can be adapted manually to low-light by increasing the exposure in real time. When the camera exposure was manually optimized to perform in the Dark condition, the crack was visible in the images with a 15 cm (6 in.) camera distance, as seen **Error! Reference source not found.**. In the Normal ondition, the crack was visible in the image taken at 20 cm (8 in.) away from the test-piece. In the Bright condition, the maximum camera distance to see the crack visually was 25 cm (10 in.) as seen in Figure 14. The required camera distance to detect the crack was 15 cm (6 in.) or less for the Dark condition, 20 cm (8 in.) or less for the Normal condition, and 25 cm (10 in.) or less for the Bright condition. The camera distance could be increased to 35 cm (14 in.) in the Normal condition and 40 cm (16 in.) in the Bright condition without the crack becoming undetectable.

Figure 12. Normal Condition, 20 cm (8 inches), GoPro, Fatigue Crack Visible

Figure 13. Dark Condition, 15 cm (6 inches), DJI Mavic, E007

Figure 14. Bright Condition, 25 cm (10 inches), DJI Mavic, E007

Nikon Camera

The Nikon camera was also not able to capture images with a visible fatigue crack in the Dark condition, E008. In the Normal condition, the Nikon detected the crack when the camera distance was up to 30 cm (12 in.), as shown in Figure 15.. In the images taken in the Bright conditon, the crack was not visible due to the light reflection in the captured images. These findings show the Nikon is best for use in the Normal lighting condition with maximum camera distance of 30 cm (12 in). Note that this is without using the zoom capability. With zooming (up to 32x optical), the camera could be considerably further away.

Findings

The results of this section indicate that visual fatigue crack detection from the captured images in the Dark condition is very difficult. Therefore, performing crack detection under a bridge will likely require the use of a light source. The Normal lighting condition was the optimum condition for both GoPro and Nikon cameras. The DJI Mavic camera performed better in the Bright condition, but its performance in the Normal condition was acceptable. The DJI Mavic and Nikon cameras took considerably better images compared to the GoPro. A GoPro camera, with the mentioned specification, is not recommended for under-bridge inspection with detailed defects (i.e. steel surface cracks). The results of this experiment are presented in Table 10.

Figure 15. Normal Condition, 30 cm (12 inches), Nikon, E008

Table 10. Minimum Requirements for Each Camera to Detect the Fatigue Crack

Camera	Lighting Condition	Required Camera Distance (C), cm (inch)
	Dark	No Detection
GoPro	Normal	10 cm (4 in) <C< 20 cm (8 in)
	Bright	No Detection
	Dark	C< 15 cm (6 in) (With Exposure Adjustment)
DJI Mavic	Normal	C< 20 cm (8 in) (No Exposure Adjustment)
	Bright	C<25 cm (10 in) (No Exposure Adjustment)
	Dark	No Detection
Nikon	Normal	C<35 cm (12 in)
	Bright	No Detection (Flashlight)

Inspection in a Controlled Environment

The second portion of this task was to simulate a bridge inspection in a controlled environment (E009 through E011). In these experiments, there was no wind, but the environment was GPS-denied and the vibrations from the UAS were introduced to the images. Using three UAS, several images were taken from indoor structures of the SMASH lab with the test-piece attached to them in different locations. The three different UAS were flown in the lab to inspect the fatigue crack in a GPS-denied environment.

3DR Iris Indoor Inspection

The GoPro camera took pictures of the test piece in the lab from the 3DR Iris, E009. The test piece was attached to a steel frame. The Normal condition was replicated roughly by having the lights on in the lab. The 3DR Iris was not stable since it does not have obstacle avoidance or altitude hold features when GPS is denied. The pilot had to stay within a safe distance of the target during the flight to prevent a collision. The closest the pilot was able to safely and stably fly the UAS was within approximately 50 cm (20 in) of the test-piece), which is more than twice that of the required camera distance obtained in the previous section. Figure 16 shows the picture taken by this UAS in the Normal lighting condition and the crack is not visible. The inspection results in the Bright and Dark conditions were also unsuccessful.

DJI Mavic Indoor Inspection

The performance of the DJI Mavic was evaluated in two scenarios: the Normal lighting condition with the test-piece attached on a horizontal steel beam approximately 3 m (10 ft) from the ground and the Dark condition with the test-piece attached to the roof frame, E010. Figure 17 shows the image of the test-piece taken by this UAS in the Normal condition. The obstacle avoidance in the UAS does not allow the pilot to get closer than 60 cm (24 in.). However, the UAS was very stable in the GPS-denied condition without turning on the obstacle avoidance feature. The sonar altitude hold feature was used to stabilize the UAS so the pilot could get approximately as close as 20 cm (8 inches) to the test-piece while the camera was at 2X zoom. The crack is clearly visible in the captured image when viewed on a desktop. In addition, the crack was visible during the inspection in FPV in real-time. The FPV video was viewed on an iPhone6 screen (12 cm [4.7 in.]) by a spotter with the pilot.

For a more realistic situation, the test-piece was attached to one of the roof frames of the SMASH lab. The lighting condition was dark and the distance between the pilot and the UAS was approximately 10 m (30 ft), which affected how comfortable the pilot was with the navigation. Figure 18 shows an image of the test-piece taken in the described situation. The camera was set to take images in a low lighting condition by changing the exposure. In addition, the 2X digital zoom option was used to compensate for the 30 cm (12 in.) camera distance, which was the closest the pilot was comfortable navigating the UAS to the target from so far way. The crack was not detectable in FPV view since the screen did not have enough resolution or size, but one can identify the crack after the inspection by looking at the pictures on a bigger monitor with higher quality. A high definition screen on a tablet would likely be adequate to see the crack in real-time.

Goose Indoor Inspection

Similar to the 3DR Iris and the DJI Mavic, the Goose was flown in the SMASH lab, E011. The test-piece was attached to the horizontal steel beam 3 m (10 ft) from the ground. The Goose was equipped with the Nikon camera as the main visual sensor and a flashlight as a lighting source. The closest camera distance for a safe inspection was roughly 70 cm (30 in.), therefore the research team zoomed the camera prior to the flight. The vehicle vibrations had a more severe effect on the captured pictures' quality due to the use of zoom feature. Figure 19 shows the picture taken by the Goose in the Normal

condition. Slight vehicle vibrations blurred the captured images considerably. The UAS, however, was able to provide several pictures in which the fatigue crack was detectable.

Figure 16. Photo of the Test-Piece Taken by 3DR Iris in the SMASH Lab, E009

Figure 17. Photo of the Test-Piece Taken by DJI Mavic in the SMASH Lab, Normal Condition, E010
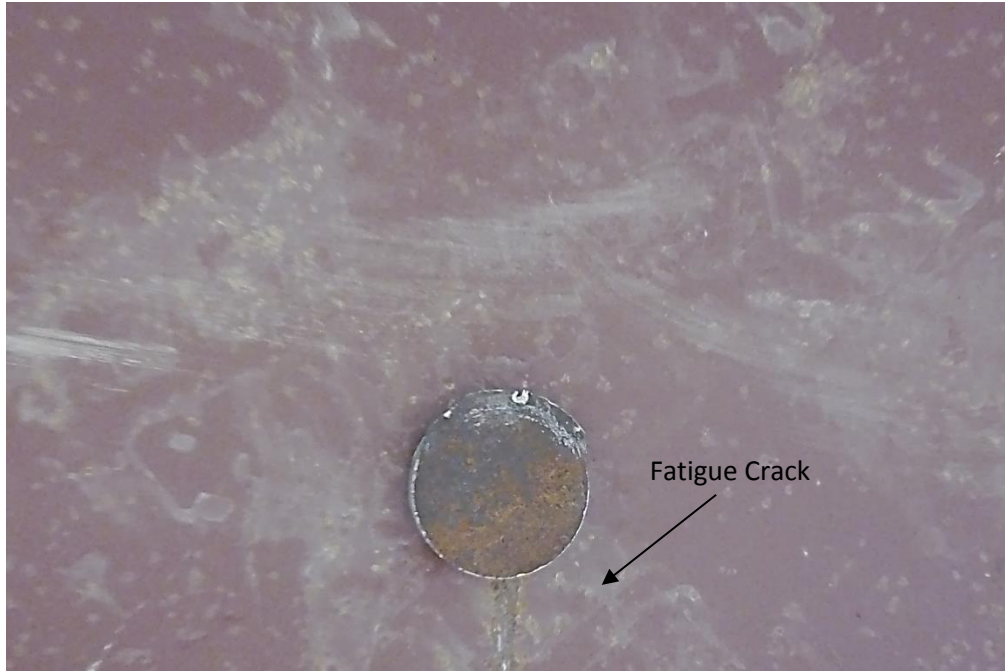
Figure 18. Photo of the Test-Piece Taken by DJI Mavic in the SMASH Lab, Dark Condition, E010

Figure 19. Photo of the Test-Piece Taken by the Goose in the SMASH lab, Normal Condition, E011

Indoor Inspection Conclusion

The SMASH lab inspections, E009, showed that the 3DR Iris, equipped with a GoPro camera, is not a proper tool to aid bridge inspectors in detecting fatigue cracks. Lack of obstacle avoidance and altitude hold features in this UAS prevents the pilot from safely getting close enough to the target to meet the required camera distances for visual fatigue crack detection. Neither zoom nor image enhancement options are offered by the GoPro camera, which makes fatigue crack detection unlikely. The 3DR Iris, with specified configurations, is not recommended for fatigue detection in bridge inspections. The GoPro camera, as noted in the previous section, is also not recommended for inspection purposes.

The DJI Mavic benefits from obstacle avoidance features (sonar and image based) and non-GPS aided altitude hold features, which were a significant aid for UAS stabilization during the flight (E010). It can be maneuvered in a confined environment, such as between the girders of a bridge, due to its small size and sufficient stability. The obstacle avoidance features can prevent the UAS from getting too close to objects, which could cause issues when trying to get very close to see a defect. However, the required camera distance can roughly be achieved in a windless environment even without turning the obstacle avoidance on. The onboard camera of the DJI Mavic can adapt to different lighting conditions, including the Dark condition, by changing the exposure. It also benefits from a 2X digital zoom which increases the chance of fatigue crack detection in real-time. These features allow the camera to capture images in which the crack is detectable when viewed on larger and higher definition screens during or after the inspection. Of the UAS tested, the research team recommends the DJI Mavic with specified configurations for fatigue crack detection in bridge inspections, especially in areas with limited space. The DJI Mavic images were clear enough to identify the crack in the Normal condition in real-time.

The Goose provided acceptable images where the crack was detectable after the inspection, however, the UAS vibrations decreased image qualities considerably (E011). This will be an issue in all UASs when using zoomed cameras. The UAS's lack of autopilot features in absence of GPS signals forced the pilot to increase the camera distance, therefore the camera had to be zoomed-in to capture images with detectable cracks. Zooming magnified the effects of mechanical vibration and led to blurry images, but adequate images could still be obtained. The minimum achieved camera distance during the inspection was roughly 70 cm (30 in.) which was more than twice the required camera distance. The use of the Goose for fatigue crack detection was successful, but requires a skilled pilot and open space for the flight. Table 11 shows the achieved camera distance by each UAS and the result of crack detection.

Table 11. Inspection Results of the SMASH Lab Simulations

UAS	Lighting Condition	Achieved Camera distance	Detection in FPV (Realtime)	Detection in Monitor (Postmortem)
3DR Iris	Normal	50 cm (20 in.)	No Detection	No Detection
DJI	Normal	20 cm (8 in.)	Detection	Detection
Mavic	Dark	25 cm (12 in.)	No Detection	Detection
Goose	Normal	70 cm (30 in.) (with 10X optical zoom)	Not Available	Detection

Outdoor Bridge Inspections

After the inspections in the SMASH lab, the research team tested UAS under a bridge to simulate real inspections, E012 and E013 (refer to appendix A). The test-piece was attached to girders of a bridge located on the west side of the Utah Water Research Laboratory at Utah State University. The aerial photo of the bridge is shown in Figure 20. The UASs were flown under this bridge, taking pictures of the test-piece with the purpose of fatigue crack detection on S001. This section represents the results of these inspections. The test-piece was placed on an interior girder and a light source used to provide different levels of illumination.

Figure 20. The UWRL Bridge

3DR Iris Outdoor Inspection

The results in the SMASH lab indicated this UAS was ineffective in fatigue crack detection, but the inspection was carried out on the UWRL bridge for a comparison, E012. The wind speed was reported at 32 km/h (20 mph) with maximum gust speed of 45 km/h (28 mph).[28] Figure 21 shows the daily temperature of the inspection day reported by KUTLOGAN25 weather station located 3.5 km (2.2 mi) away from the inspection location. Figure 22 and Figure 23 provide information about the wind direction and wind and gust speed, respectively, from the same weather station. As expected, the 3DR Iris and GoPro camera were unable to provide images with sufficient quality for fatigue crack detection. The feasible camera distance was roughly 60 cm (24 in.) since the UAS was dangerously moving with the wind and could not be controlled. Figure 24 shows the image of the test-piece taken by this UAS in the Normal lighting condition. This image, and others like it, is unacceptable for nearly any kind of inspection.
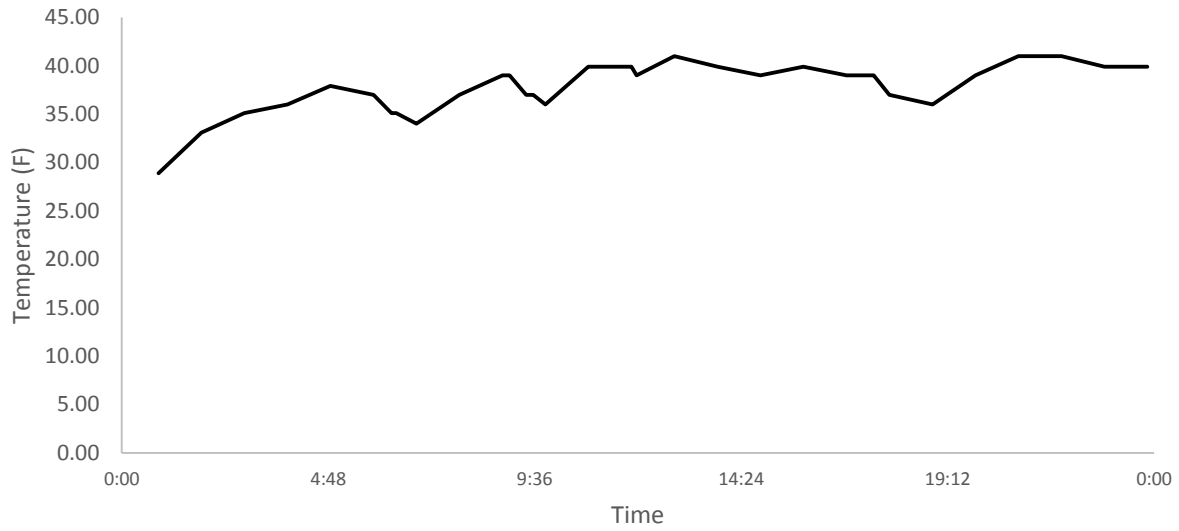
Figure 21. Daily Temperature from January, 10, 2017 at the UWRL Bridge from KUTLOGAN25 Station[28]
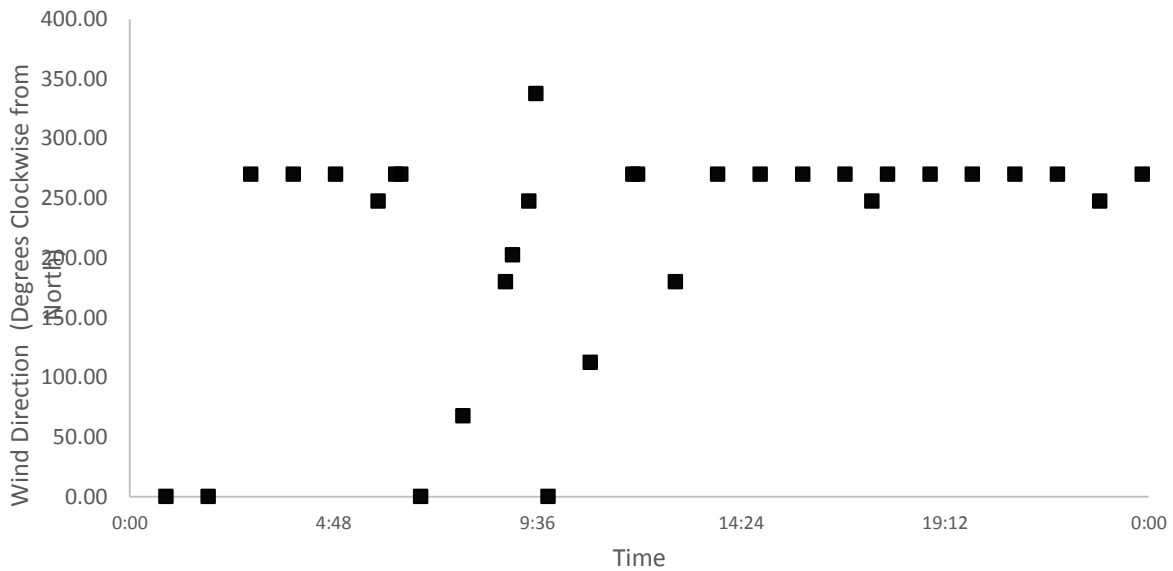
Figure 22. Wind Direction from January, 10, 2017 at the UWRL Bridge from KUTLOGAN25 Station[28]
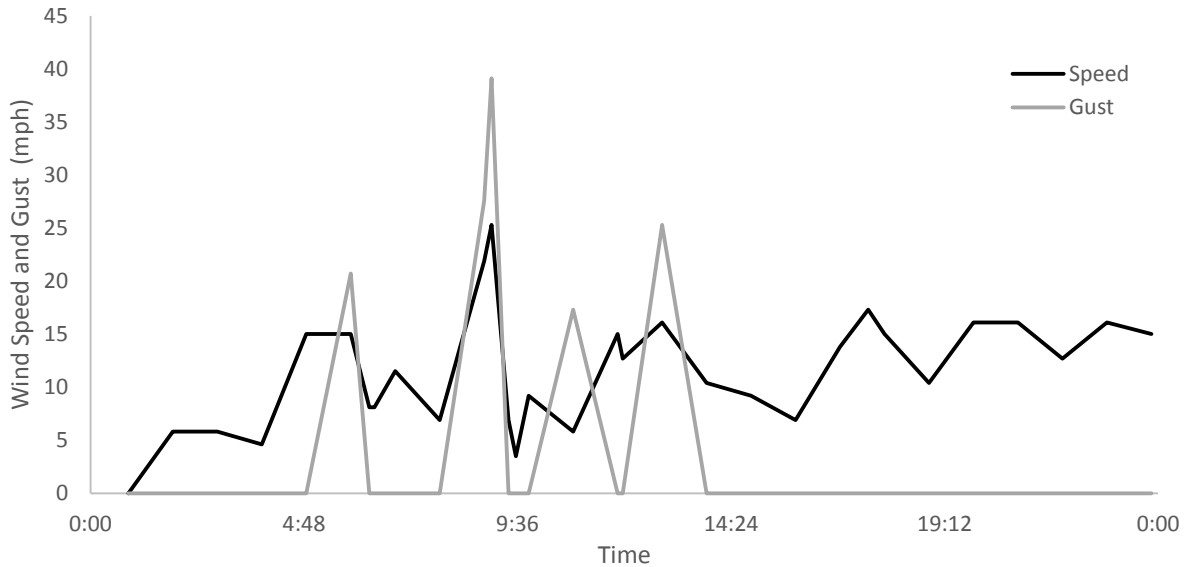
Figure 23. Wind Speed and Gust Information from January 10, 2017 at the UWRL Bridge from KUTLOGAN25 Station[28]

DJI Mavic Outdoor Inspection

The DJI Mavic was used to inspect the bridge on the same day as the 3DR Iris, E013. Despite the wind, the UAS was flown approximately 25 cm (10 in.) away from the test-piece which was close enough for the inspection purposes. The UAS's stability in the gusting wind was adequate, capturing several images in which the fatigue crack was visible during the inspection (real-time in FPV and post-processing). By changing the exposure and focus features in the camera, the fatigue crack was visible in the Normal and the Bright lighting conditions in real-time, as shown in Figure 25 and Figure 26, respectively. The research team placed the test-piece in a very dark location under the bridge with surface illumination of 5 lx and several images were taken with the maximum exposure setting on the camera. It was not possible to see the crack in FPV during the inspection, but the crack was visible in the images after viewing them on a desktop monitor, as seen in Figure 27. With a larger FPV monitor, like a tablet, real-time detection is likely. The test-piece was also attached on a girder bottom flange to determine the camera angle effects on the crack detection. Although the fatigue crack was not detectable in real-time, one can review the captured images on a bigger monitor to see the fatigue crack. One of these images is shown in Figure 28. This image is significant considering that the tilt-angle of the camera on the DJI Mavic is limited to 30 degrees.

Figure 24. Photo of the Test-Piece Taken by 3DR Iris, UWRL Bridge, Normal Condition, E012

Figure 25. Photo of the Test-Piece Taken by DJI Mavic, UWRL Bridge, Normal Condition, Normal Camera Angle, E012

Figure 26. Photo of the Test-Piece Taken by DJI Mavic, UWRL Bridge, Bright Condition, Normal Camera Angle, E012

Figure 27. Photo of the Test-Piece Taken by DJI Mavic, UWRL Bridge, Dark Condition, Normal Camera Angle, E012

Figure 28. Photo of the Test-Piece Taken by DJI Mavic, UWRL Bridge, Bright Condition, Oblique Camera Angle, E012

The DJI Mavic can be used for fatigue crack detection successfully. This UAS provides detailed images in all lighting conditions at distances as far as 25 cm (10 in.), often in FPV in real-time, but certainly on a large monitor after the inspection.

Goose Outdoor Inspection

The bridge clearance was less than 2 m (6.5 ft), which is too close to the ground and water for VTOL UAS with the power of the Goose, where ground effects would affect flight stability. The Goose would need at least 2.5 meters, plus additional space for maneuvering, so the Goose was not tested under the bridge.

Outdoor Inspection Conclusions

The outdoor bridge inspection experiments showed that the 3DR Iris is an ineffective UAS for fatigue crack detection under the bridge due to both camera and vehicle weaknesses, E012. The camera lacked exposure adjustments, focus, and zoom features. The UAS was affected by windy conditions, which decreases the quality of the captured images. GoPro cameras are commonly used with UASs, however, they are not recommended to detect fine defects in under-bridge inspections. In addition, the UAS was very sensitive to the wind and acted particularly unstable, reducing safety for the UAS and pilot.

The DJI Mavic showed promising results for fatigue crack detection in both real-time and post-inspection (E013). The camera was able to capture pictures with good detail in the Normal and the Bright conditions since the exposure and focus of the camera can be adjusted for clearer images of the fatigue

crack. The 2X digital zoom allowed the UAS to maintain a safe distance while capturing these pictures. The UAS was stable without using obstacle avoidance and captured high quality images. The camera's performance in the Dark condition was also successful and the crack was visible in this condition. The camera's vertical rotation is limited to 30 degrees, which can make upward inspections challenging, but images taken from the test-piece demonstrated the ability of this UAS to be used for fatigue crack detection when the camera's point-of-view is not orthogonal to the test-piece.

The Goose could not be tested under the UWRL bridge because there was not enough vertical clearance between the ground and bridge. Lack of free space around the UAS can cause it to lose stability due to ground effect turbulence. Ground effect turbulence is the increased lift force and decreased drag that is experienced when the rotors are too close to the ground, and the associated turbulence, adversely affects manual and automated control.

The DJI Mavic was as an effective tool for fatigue crack detection in the outdoor inspections. This UAS is the most stable without GPS and holds position in in strong winds. The built-in camera on this UAS can capture images where the crack is detectable even in different lighting conditions by adjusting the light exposure, which is critical for low-light scenario. The camera's small size allows the DJI Mavic to fly in confined environments, while the stability of the UAS gives the minimum possible camera distance among three tested UASs.

Table 12 summarizes the level of success each UAS had with fatigue crack detection in different lighting conditions under the UWRL bridge using a subjective rating system of good, fair or poor.

Table 12. Subjective UAS's Performances Under the UWRL Bridge

UAS	Camera	Minimum Safe Camera Distance	Dark	Normal	Bright
3DR Iris	GoPro Hero 4	60 cm (24 in.)	Poor	Poor	Poor
DJI Mavic	On Board DJI	25 cm (10 in.)	Fair	Good	Good

Autonomous Fatigue Crack Detection

The captured images in previous sections can be analyzed using image processing techniques for autonomous or semi-autonomous crack detection. The texture of the test-piece was a major obstacle for any autonomous detections (as it was for visual inspection), thus several edge detection techniques were implemented in a computer program (see Appendix C) and tested on the images taken from E014 (other images were attempted, only those from the DJI Mavic were successful) to determine the level of success of each technique. See Table 13 for the level of success of each detector. The most successful method was the Laplacian of Gaussian (LoG) edge detector. The proposed algorithm included applying a LoG filter on the captured images. The resultant image after applying the LoG filter was an image with intensified edges. This image is called the edge image. Then, the edge image was converted to a binary image, with 1s assigned to the detected edge pixels and 0s to everything else. The detected edges were then superimposed on the original image for comparison and visual augmentation. The execution time of the LoG program was less than 1 second per image which would allow inspectors to use this algorithm in near real-time inspections.

Table 13. Performance of the Implemented Edge Detectors on E014

Edge Detector	Average Detected crack's length (%)	Level of success
Canny	25	Poor
Sobel	55	Medium
LoG	> 80	Good
Roberts	20	Poor
Gaussian High-pass filter	< 10	Poor

Image Processing Using the 3DR Iris Photographs

The images captured by this UAS did not represent the fatigue crack as strong edges, thus, the proposed algorithm failed to detect the crack. The only edges detected from this UAS images were the edges of the test-piece itself.

Image Processing Using the DJI Mavic Photographs

The image processing results were successful on the images taken by the DJI Mavic in the SMASH lab. The image shown previously in Figure 17 was processed by the proposed LoG filter. In the final image, the fatigue crack was detected along with the edges of the test-piece, as seen in Figure 29. In practice, the edges of the test-piece do not exist and the algorithm will detect only the fatigue crack along with some surface clutter. The LoG algorithm was able to detect the majority of the crack length in this figure.

The same algorithm was executed on the images taken by DJI Mavic during the UWRL bridge inspection. Figure 30 shows the result of the crack detection method on one of the images taken during the UWRL bridge inspection, previously shown in Figure 26. The edges of the test-piece and its shadow border were picked in the final image, and most of the crack's length was also detected. Additional filtering can remove the detected edges from the test-piece and shadow edges.

Image Processing Using the Goose Photographs

The images taken by the Goose in the SMASH lab were not clear enough because the UAS's vibrations were amplified by the optical zoom. Therefore, the proposed algorithm was unable to detect the fatigue crack autonomously in these images, even though the crack was visible to the human eye. Only the edges of the test-piece were reported as the major edges in the resultant images, since they consisted of stronger pixel intensity gradients compared the fatigue crack.

Figure 29. The Detected Crack Using Image Processing Techniques on the SMASH Lab Images (Laplacian of Gaussian), E014
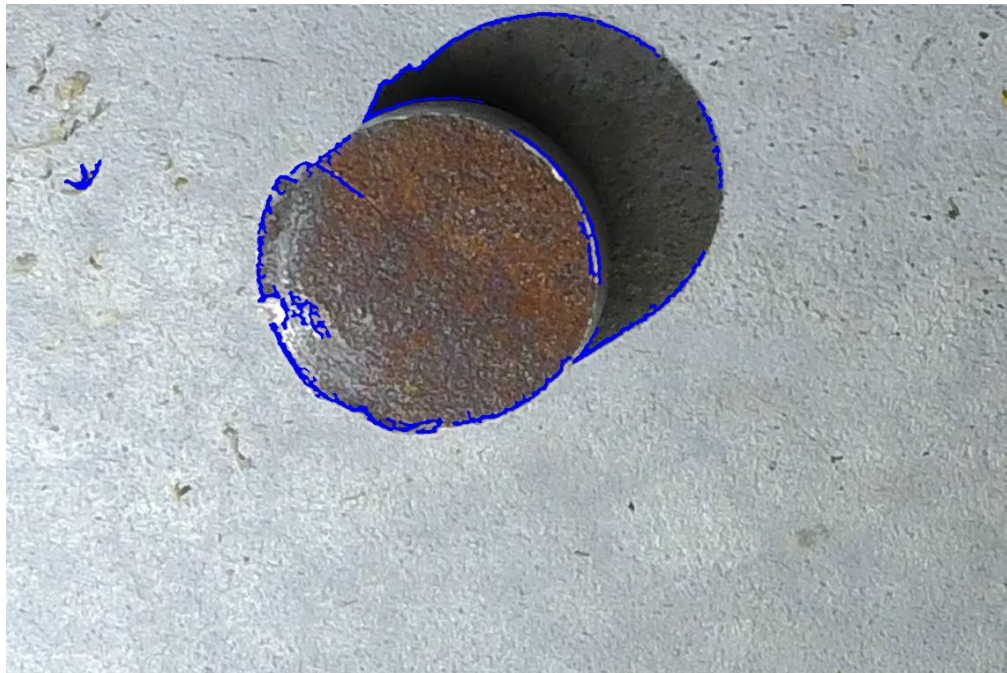

Figure 30. The Detected Crack Using Image Processing Techniques on the UWRL Lmage (Laplacian of Gaussian), E014

Autonomous Fatigue Crack Detection Conclusion

The research team proposed an image processing technique to find the fatigue cracks autonomously in the captured images by three UASs, E014. The 3DR Iris and the Goose images did not present the fatigue crack as a strong edge nor did it capture the crack at all, therefore, the proposed method was unable to locate the crack in their images. The pictures captured by the DJI Mavic worked better with the algorithm and the fatigue crack was detected, along with the edges of the test-piece. The research team expects that the LoG fatigue crack detection method will detect cracks most effectively on structures with similar crack sizes as the test piece since the edges of the test-piece will not interfere with the crack detection results. This technique is likely most useful as an augmentation tool for inspectors and has the potential to be used in near real-time.

Passive Thermal Fatigue Crack Detection

In theory, the presence of surface cracks changes emissivity of any surface. Thermal cameras read surface emissivity in different locations and convert them into temperature by taking several parameters into account.[26] Difference in emissivity values in locations with surface cracks cause discontinuity in surface temperature distribution and can be used to detect defects in thermal images. Thermography can be carried out with an external heating and cooling source (active) or without an external heating/cooling source (passive).

The previous sections showed that the achievable camera distance during UAS bridge inspection was roughly 60 cm (25 in.) to 75 cm (30 in.). To simulate the inspection of fatigue cracks using UASs, the test pieces were actively heated up by the sunlight and monitored using two thermal cameras at a distance of 75 cm (30 in.) from the two test-pieces (E015 and E018). The research team placed the test-pieces under direct sunlight for a few hours and then monitored the heat loss of the test-pieces from both sides (A and B, see Table 14) after removing them from direct sunlight. The research team analyzed all images after the experiment using ThermaCAM Researcher Software for better crack detection. [29]

The first thermal camera was a FLIR SC 640 with 1°C sensitivity. The research team selected this camera because it had similar sensitivity to conventional thermal cameras compatible with most commercial UASs, E015 and E016. Figure 31 and Figure 32 show the thermal images taken from the first and second test-piece, respectively, while they were losing heat. As seen in the thermal images, fatigue crack detection was not achieved with this method.

The research team repeated the experiment using an FLIR E8 camera that has 0.2°C sensitivity to conduct experiments E017 and E018. Figure 33 shows the captured thermal image from the side A of the first test-piece. The crack, located in the 8 o'clock orientation, was not explicitly detected in the thermal image. However, a cold region can be detected around the crack location.

Table 14. Fatigue Crack Specimen Side Designation

Specimen	Side A	Side B
S02		
S03		
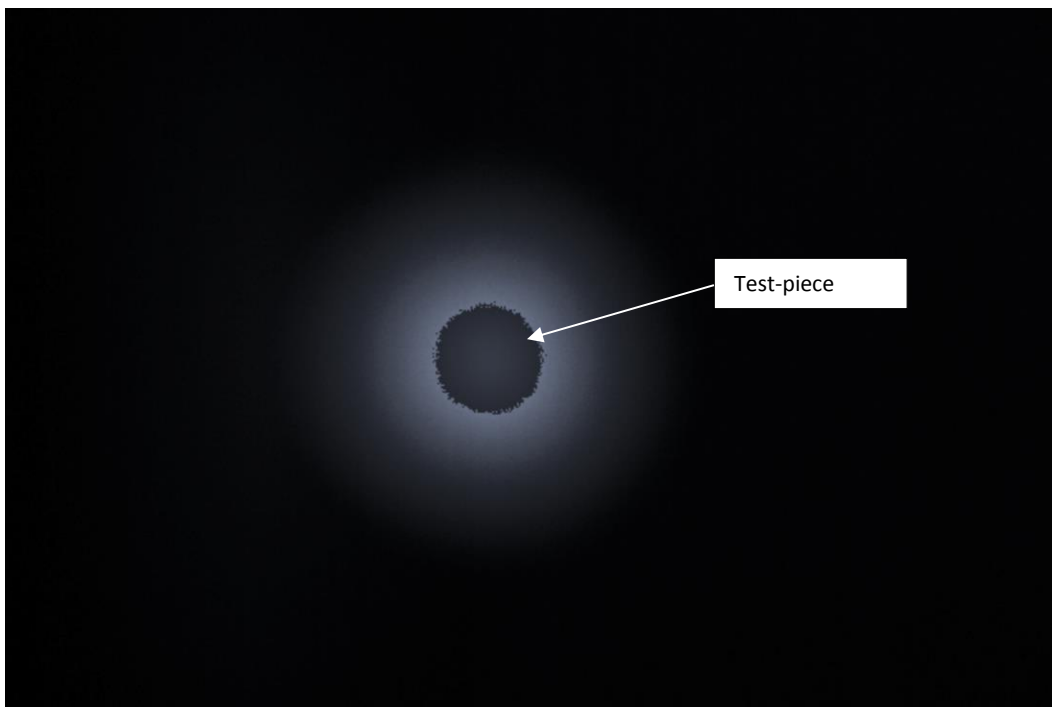
Figure 31. Thermal Image from the First Test-Piece, Passive, E015

Figure 32. Thermal Image from the Second Test-Piece, Passive, E016

Figure 34 is an image taken of the side A of the second test-piece while it was losing heat. The image has a temperature gradient of 35°C (64°F). The fatigue crack on this specimen was deeper, thicker, and longer than the first test-piece, separating the test-piece into two regions: cold and warm. The crack was located at the boundary of these two regions and can be detected in the thermal image. Although the crack detection in the second test-piece was more successful than the first one, the temperature distribution may have been affected significantly by the yellow paint strip.
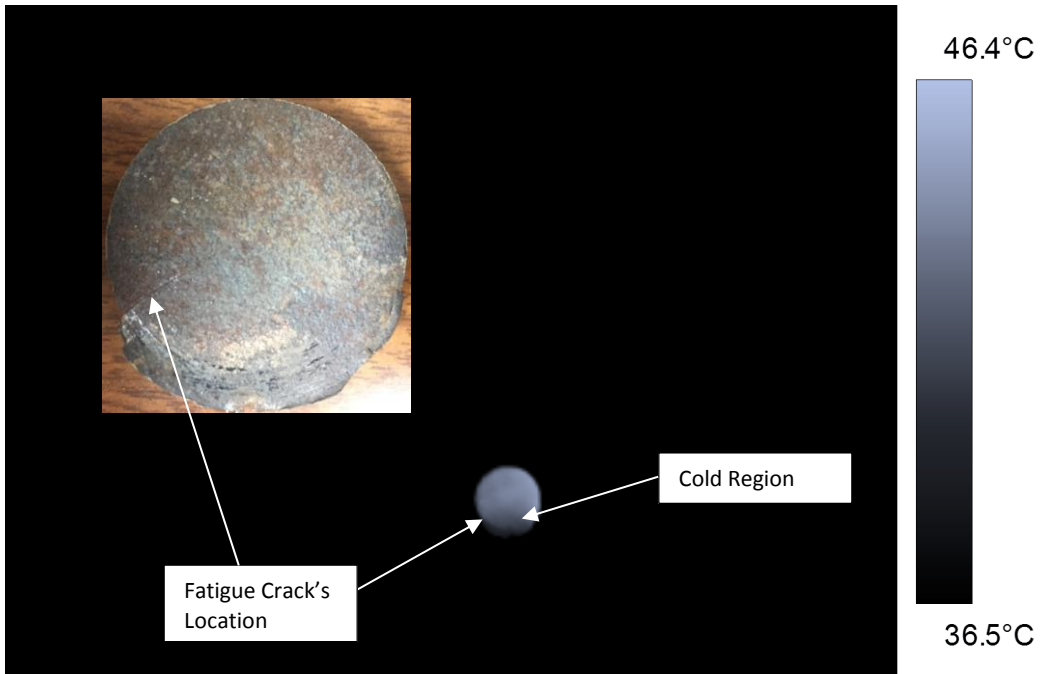
Figure 33. Thermal Image of the Side A of Test-Piece 1, 75 cm (30 in) Camera Distance, E017
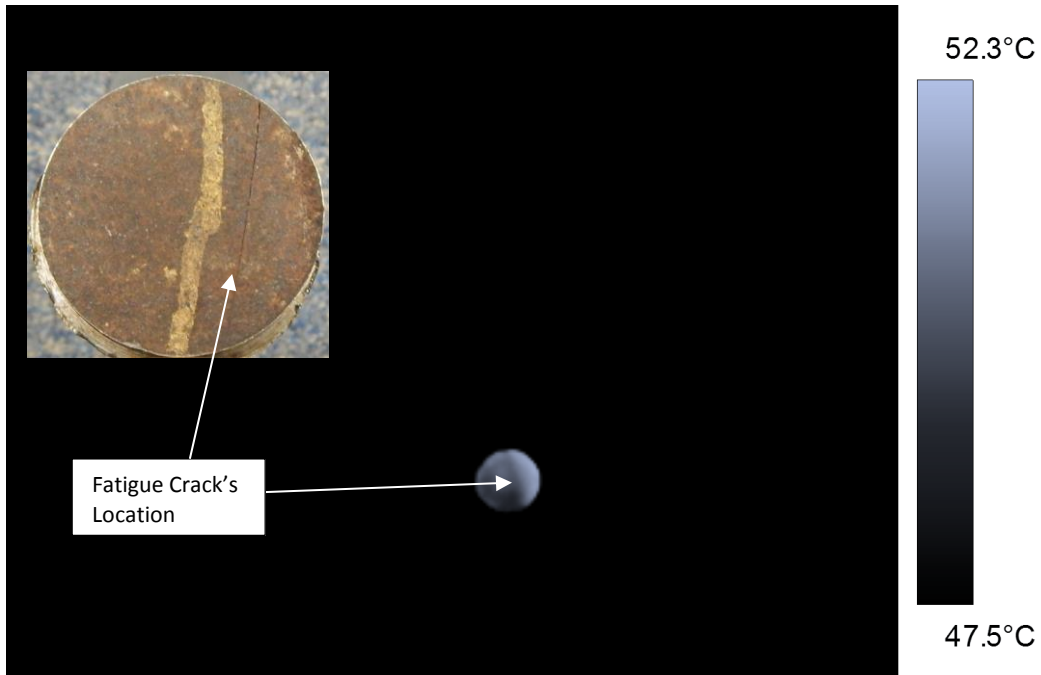
Figure 34. Thermal Image of the Side A of Test-Piece 2, 75 cm (30 in) Camera Distance, E018

Active Thermal Fatigue Crack Detection

This section provides the results of active thermography to detect the fatigue cracks on test-pieces, experiments E019 and E020. Each test-piece was attached to a mount by a magnet. The heat-gun was placed on one side of the examined specimen while the thermal camera, mounted on a tripod with 5 cm (2 in.) distance to the test-piece, monitored the other side of it. Once the temperature on the monitored surface reached to roughly 275°C (530°F), the heat gun was turned off and the thermal camera took pictures while the test-piece lost heat at 5-second intervals. In the figures below, the image most effectively exhibiting the fatigue crack is presented. The camera's distance from the specimen was much smaller and temperature gradients were higher in this set of experiments than the passive case (which was simulating a UAS inspection). The distance between the thermal camera and the test-pieces was 5 cm (2 in.). The thermal camera monitored each side of each test-piece after the other side was heated by the heat gun in the lab. The thermal camera took several thermal images of the test-piece at different temperatures, providing different temperature gradients to locate the fatigue cracks.

Figure 35 shows the thermal image taken from the side A of the first test-piece and has a thermal gradient of 93°C (167°F), E019. The passive thermal inspection of this side was unconvincing, but the crack can be seen in the close-range thermal image acquired with a higher temperature gradient. Figure 36 shows the temperature profile along a section line passing over the crack on the test-piece. The profile hit its temperature peak approximately at the crack's location since it was losing more heat than the surrounding material.

The side B of the first test-piece showed more promising results in the thermal inspection, as seen in Figure 37, E019. The fatigue crack was distinct because its thermal loss was higher than its surroundings. The cold region in this image corresponded to the visually darker region on the center of the test-piece (left inset visual image in Figure 37, which exhibits a different temperature distribution than the rest of the test piece). The temperature profile along with a line is shown in Figure 38. The fatigue crack location was consistent with a local maximum in the profile graph.

The fatigue crack on test-piece number two was easier to see visually. Thermally the crack seemed separated from the second test-piece into two parts in terms of surface temperatures when examined in experiment E020. Figure 39 shows the thermal image from the side A of this test-piece with temperature gradient of 125°C (225°F), E020. The top part of the test-piece was colder than the bottom part due to the presence of the fatigue crack, which was consistent with the passive result. The other irregularity in temperature distribution occurred in the middle of the thermal image. This was due to a paint strip on the test-piece, which also is shown in Figure 39. Figure 40 shows the temperature profile of side A of the second test-piece along with a line passing over the fatigue crack. The research team observed two temperature distribution anomalies in this figure, which were consistent with the fatigue crack and the paint strip locations. These abnormalities were presented with local extrema; the local maximum for the fatigue crack and the local minimum for the paint strip.

Finally, the thermal camera monitored side B of the second test-piece, and one can detect the fatigue crack in the thermal image with 57°C (103°F) temperature gradient, see Figure 41 (E020). Extracting the temperature profile of the test-piece along a line passing over the fatigue crack (often called a

thermogram), the fatigue crack location was consistent with an irregularity in the surface temperature distribution in Figure 42.

Figure 35. Thermal Image of the Side A of Test-Piece 1, 5 cm (2 in) Camera Distance, E019
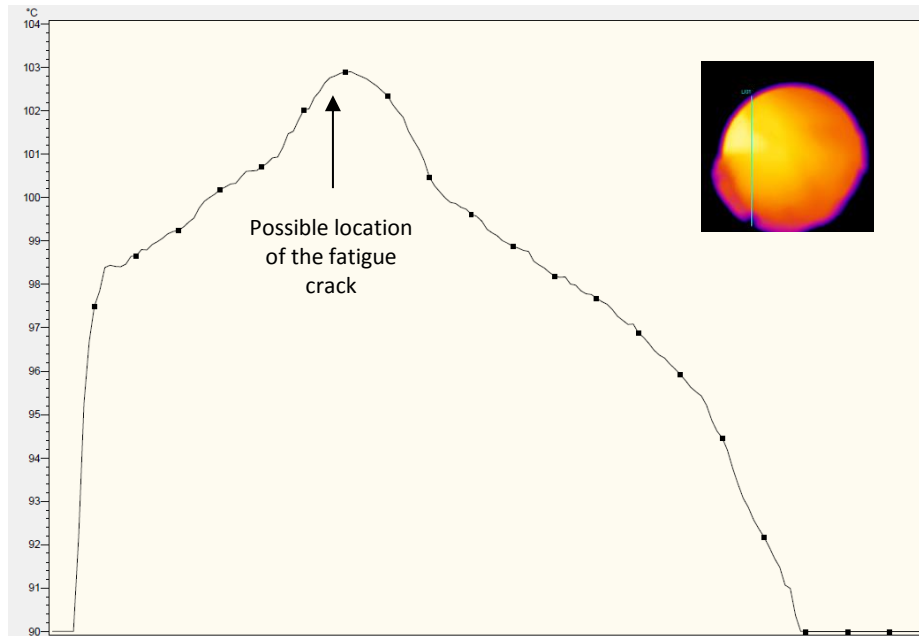
Figure 36. Temperature Along the Profile Line for the Side A of Test-Piece 1, 5 cm (2 in) Camera Distance, E019
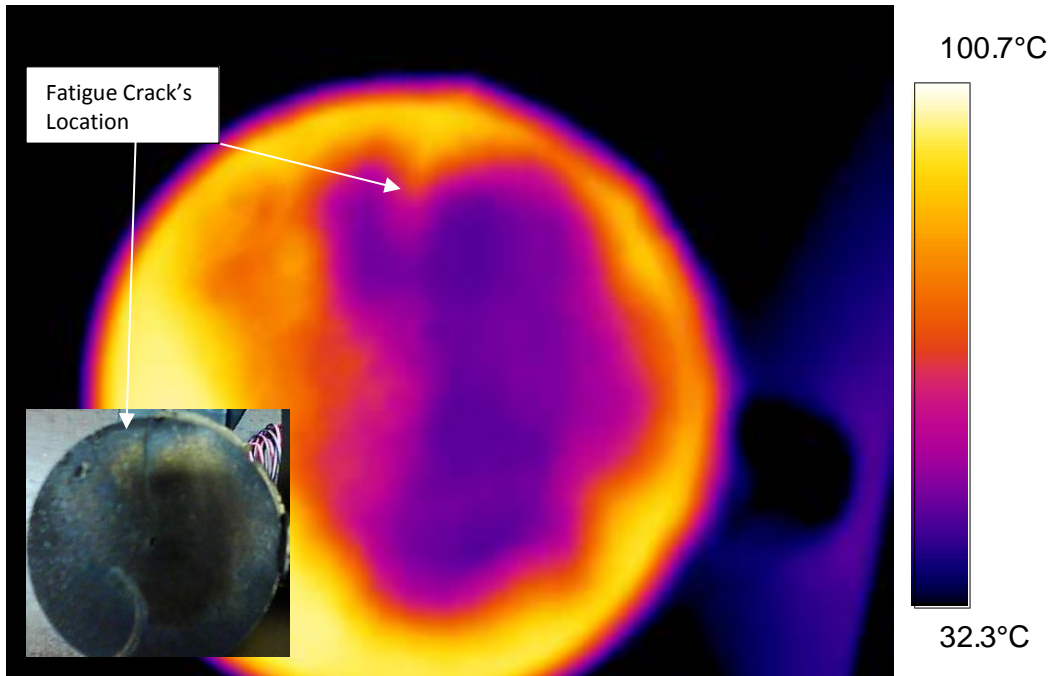
Figure 37. Thermal Image of the Side B of Test-Piece 1, 5 cm (2 in) Camera Distance, E019
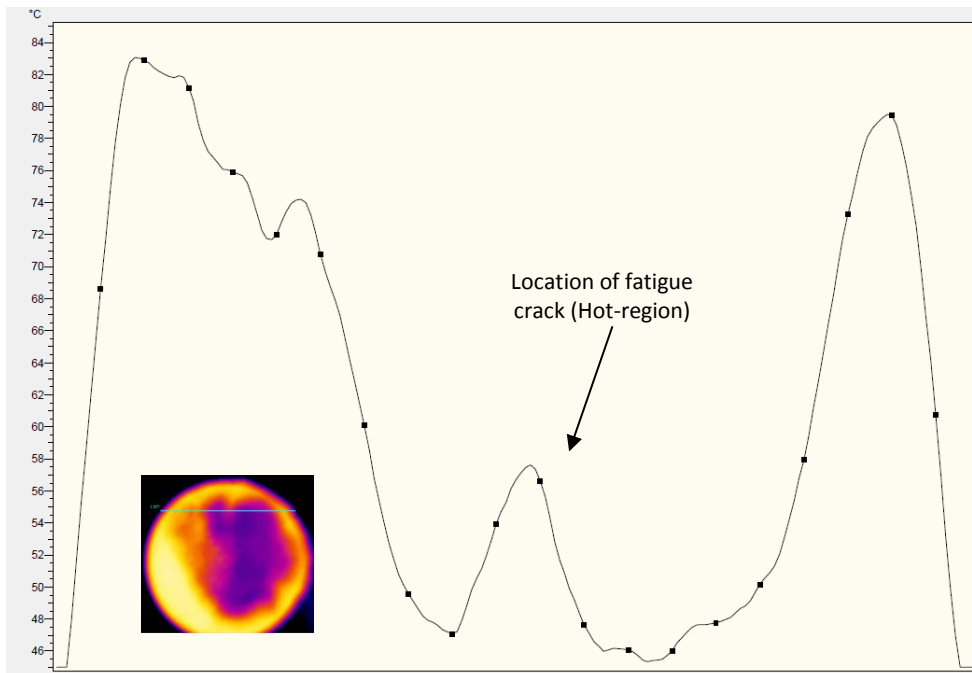
Figure 38. Temperature Along the Profile Line for Side B of Test-Piece 1, 5 cm (2 in) Camera Distance, E019
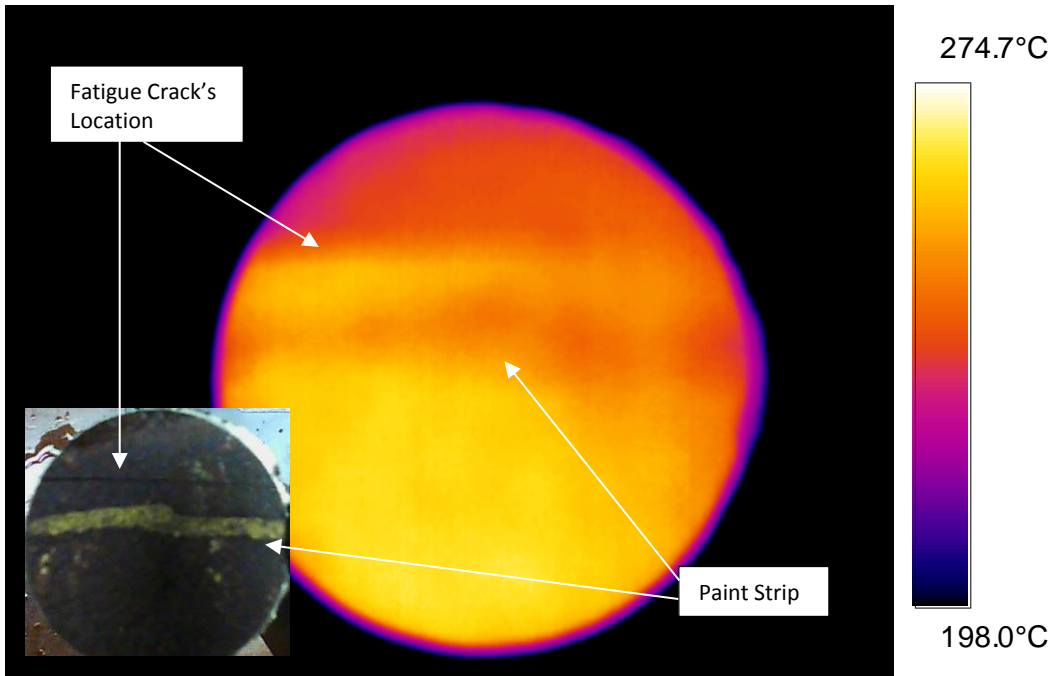
Figure 39. Thermal Image of the Side A of Test-Piece 2, 5 cm (2 in) Camera Distance, E020
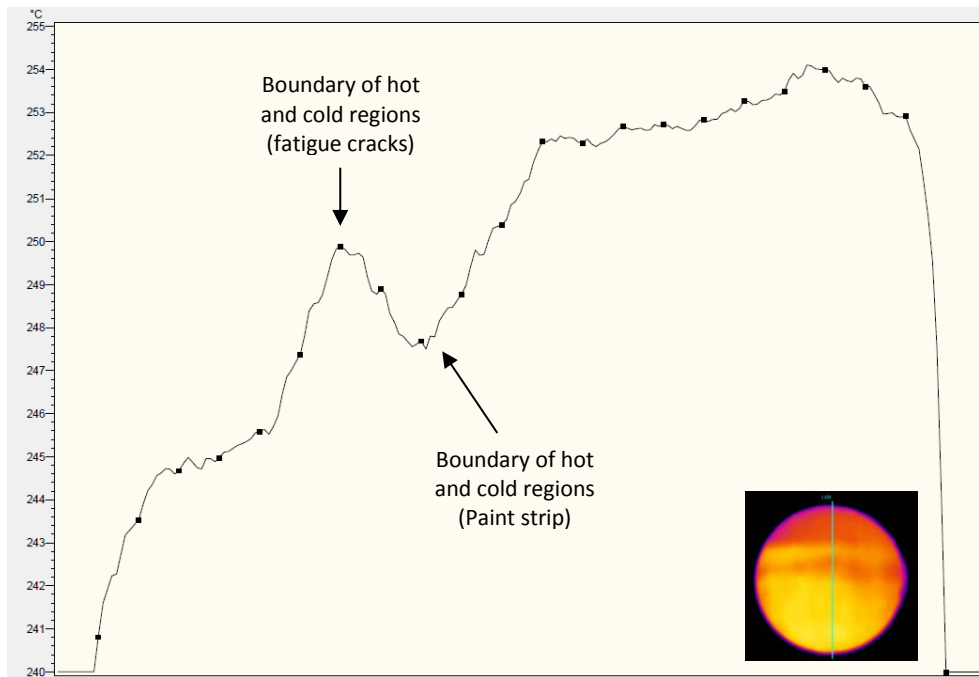
Figure 40. Temperature Along the Profile Line for Side A of Test-Piece 2, 5 cm (2 in) Camera Distance, E020
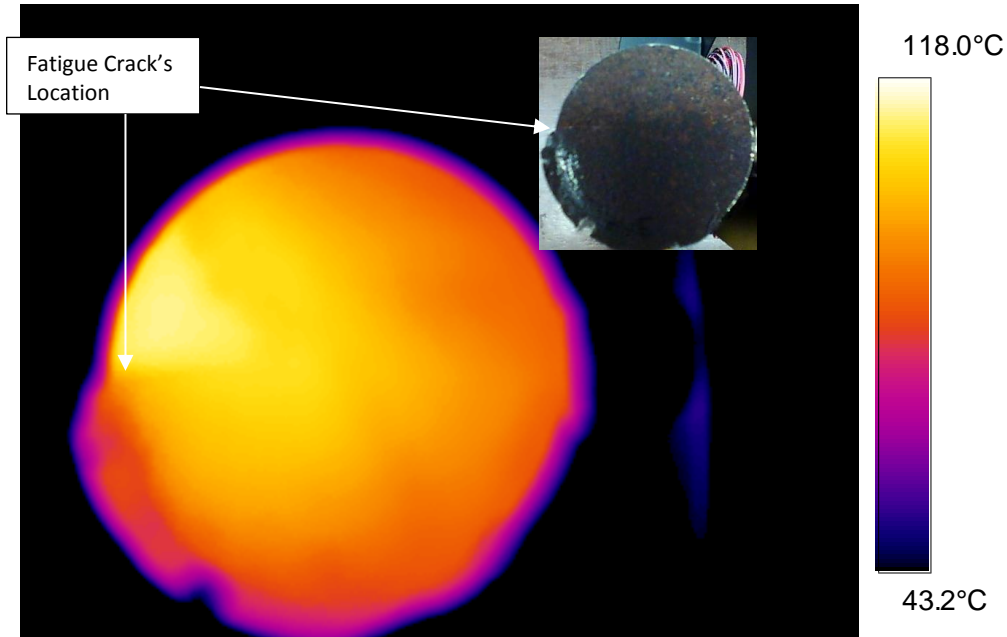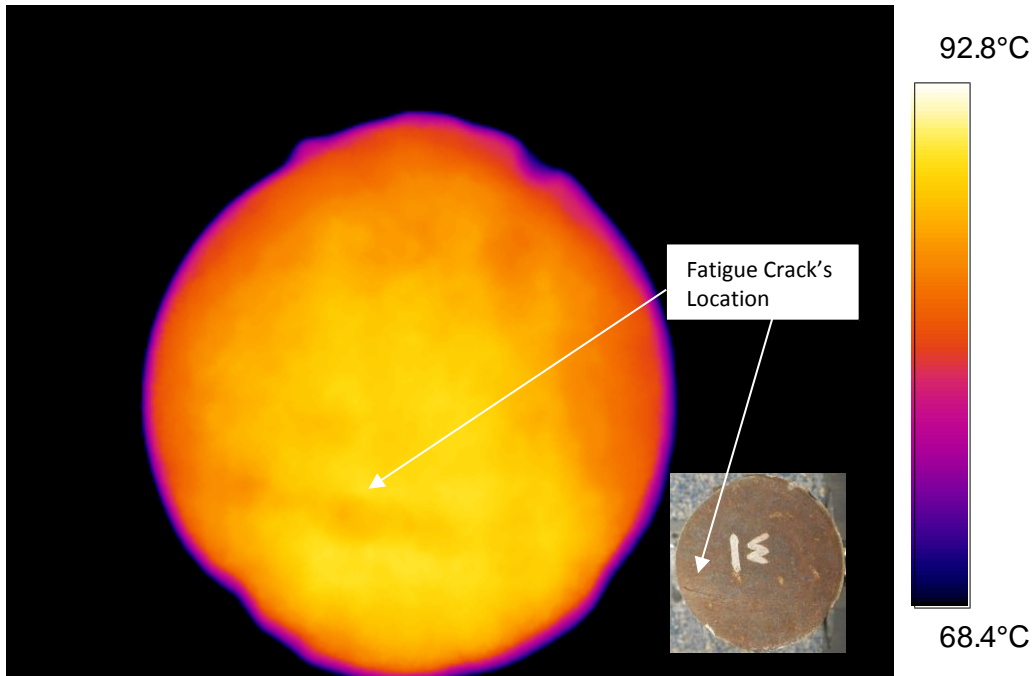
Figure 41. Thermal Image of the Side B of Test-Piece 2, 5 cm (2 in) Camera Distance, E020
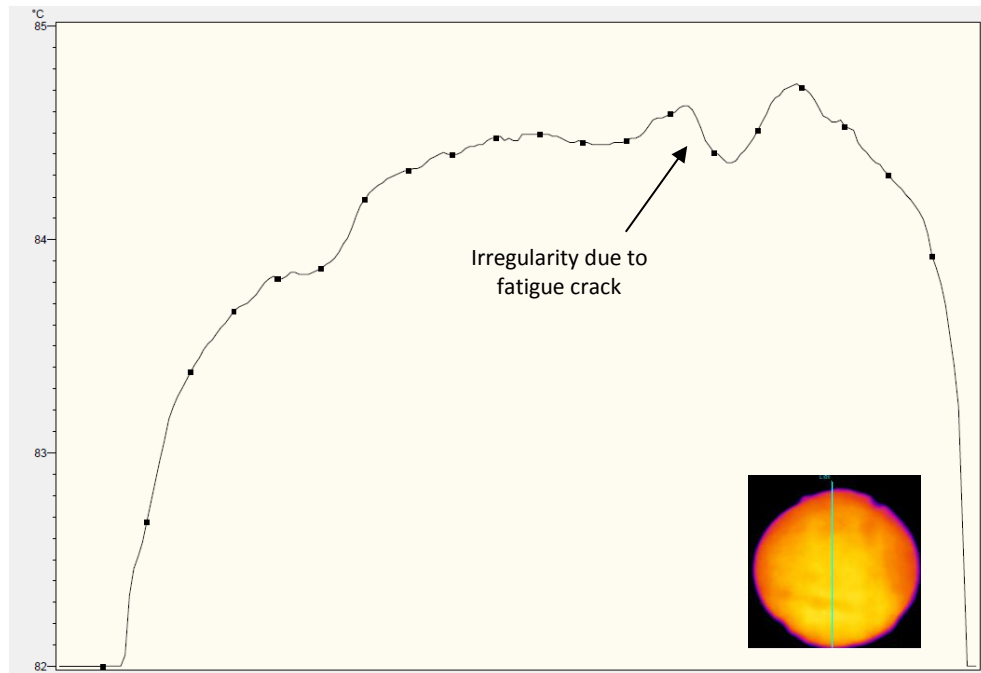
Figure 42. Temperature Along the Profile Line for the Side B of Test-Piece 2, 5 cm (2 in) Camera Distance, E020

Thermal Fatigue Crack Detection Summary

The research team investigated the feasibility of fatigue crack detection using passive and active thermography in this section. Two thermal cameras with 75 cm (25 in.) camera distance took thermal images of the test-pieces while the test-pieces were losing heat after being exposed to sunlight. Thermal images from the first thermal camera did not provide any indications of fatigue cracks due to the camera's sensitivity (+/- 1°C), E015 and E016. This camera had similar sensitivity to most thermal cameras compatible with UASs. The research team repeated the experiment using a more sensitive camera (+/- 0.2°C) in experiments E017 and E018. The results were promising, but not conclusive with the studied proximities. Therefore, the research team carried out active thermography on the test-pieces at a much closer range, E019 and E020. The test-pieces were investigated with 5 cm (2 in.) camera distance and more heat input. The active experiment results verified the passive results, suggesting the possibility of fatigue crack detection using thermal images. Table 15 presents a summary of the thermal crack detection experiments (E015-E020).

Table 15. Summary of Thermal Crack Detection Requirements

Experiment ID	Active/Passive	Specimen ID	Camera	Detection Distance, cm
E015	P	S04	FLIR SC 640	-
E016	P	S05	FLIR SC 640	-
E017	P	S04	FLIR E8	-
E018	P	S05	FLIR E8	-
E019	A	S04	FLIR E8	5
E020	A	S05	FLIR E8	5

To apply this methodology on UASs, there are certain barriers that need to be overcome. First, the pixel resolution of thermal images is usually considerably less than the visual images and the UAS must be flown very smoothly and closely to capture useful thermal images. Second, the FLIR E8 thermal camera, which provided promising results for both passive and active cases, is not mountable on UASs. UAS compatible thermal cameras with a sensitivity of +/- 0.2°C are considerably more expensive than conventional cameras due to size and weight. Third, even with an expensive and accurate camera, fatigue crack detection would likely still require active thermography, which is difficult or impossible to perform with current off-the-shelf UASs.

Controlled Fatigue Crack Detection Conclusions

In this chapter, the research team presented the investigation into the feasibility of fatigue crack detection using visual and thermal images.

The research team investigated the feasibility of fatigue crack detection using two remote sensing methodologies: visual and thermal images. Three UASs were used to capture images of a fatigue crack. These images helped the research team provide crack detection requirements, E006 through E008, in terms of lighting condition and camera distance to investigate the feasibility of fatigue crack detection in GPS-denied environments in a no wind situation and to assess the UAS-based fatigue crack detection with GPS-denied navigation under a bridge.

The requirements for fatigue crack detection using three visual cameras (not using the UASs) in terms of camera distance and lighting conditions, in *highly controlled office conditions*, were determined as follows:

- Only the DJI Mavic camera took pictures with recognizable cracks in all lighting conditions, E007.
- Based on the results from the Nikon and DJI Mavic camera (E007 and E008), minimum surface illumination of 200 lx was recommended to capture proper images, even though the DJI Mavic was successful at lower lx. It is acknowledged that this may not be feasible in all situations. UAS mounted lights, or handheld spot lights, or both can be used effectively to increase surface illumination.
- The furthest camera distance for an image with visible fatigue crack was achieved with the Nikon camera in the Normal condition: 30 cm (12 in.) in E008.

The research team used three UAS to capture images of a test-piece with a known fatigue crack. This was done in the SMASH lab using three UAS: the 3DR Iris, equipped with a GoPro camera; the Goose, equipped with a Nikon camera; and the DJI Mavic, E009 through E011. The images from this semi-realistic inspection were used to determine if fatigue crack detection using UASs is feasible. The findings from this experiment under *GPS-denied, but environmentally controlled conditions* are outlined below:

- Crack detection in DJI Mavic images was feasible in all lighting conditions, E010. Crack detection was enhanced by the DJI Mavic's superior stability, which allowed the UAS to reach a closer camera distance to the inspected piece, and the camera's exposure adjustment for darker scenes.
- The 3DR Iris, equipped with the GoPro camera, was not stable enough to provide the required camera distance in the absence of GPS signals, and therefore was not recommended for this task, E009.
- The inspection results of the Goose, equipped with the Nikon camera, allowed the detection of the fatigue crack in the test piece. The camera distance was 70 cm (35 in.) and the camera was pre-zoomed, however the images were blurry due to vibrations, E011.

The UAS were used to *inspect the test piece underneath the UWRL bridge*, to find the fatigue crack in an uncontrolled environment (E012 and E013):

- Due to 32 km/h (20 mph) wind speed with maximum gust speed of 45 km/h (28 mph) the minimum safe camera distance for the 3DR Iris was 60 cm (24 in.) in E012, which was greater than what was achieved in the SMASH lab, 50 cm (20 in.), and there was no detection in the images.
- The pilot was able to provide a similar camera distance to that in the SMASH lab experiment with the DJI Mavic, 25 cm (10 in.) in experiment E013.
- Only the DJI Mavic pictures showed the fatigue crack (E012).
- The DJI Mavic showed the fatigue crack in all lighting conditions (E012).
- The Goose was not flown due to the low camera distance of the bridge.

Table 16 presents a summary of the visual detection requirements for the fatigue crack in the test-piece using the DJI Mavic for each condition in the simulated environment under the bridge.

Table 16. Summary of Visual Fatigue Crack Detection Requirements

Location	Camera	Distance to specimen for detection (cm)	Illumination (lx)
office	GoPro Hero 4	10-20	100-250
	DJI built-in	≤ 15	20-100
		≤ 20	100-250
		≤ 25	250 and more
	Nikon	≤ 30	100-250
SMASH lab	GoPro Hero 4	none	none
	DJI built-in	≤ 20	20-100
		≤ 25	100-250
	Nikon	≤ 70	100-250
UWRL	GoPro Hero 4	none	none
	DJI built-in	≤ 25	20-100
		≤ 25	100-250
		≤ 25	250 and more
	Nikon	Not attempted	

Finding fatigue cracks using image processing techniques was feasible when the research team used the DJI Mavic to capture the images and used the LoG edge detector as the primary image processing algorithm, E013. The experiment on the UWRL bridge showed that the DJI Mavic was the best device of the three UASs to help a bridge inspector find the fatigue cracks. This UAS provides images with visible fatigue cracks, even in different lighting conditions. The 2X digital zoom and the ability to change the camera exposure enhanced the quality of the FPV real-time inspection. Also, the sonar altitude hold sensor stabilized the UAS, even during pilot described undesirable wind conditions.

The Goose, as equipped, was sufficient for finding some cracks in the laboratory, but its images exhibited much blurrier pictures, which was thought to be detrimental to the inspection process. Additionally, its control hardware, software, and size made the UAS more difficult to control compared to the DJI Mavic. The advantage of the Goose as a UAS is its payload capacity and with additional tuning of its flight characteristics, the Goose may eventually be considered feasible when additional sensors are mounted on the UAS. Overall, the limitations of the Goose were such that it did not perform on the same level as the off-the-shelf DJI Mavic.

The inspection simulations in the SMASH lab and at the UWRL bridge showed that the 3DR Iris, equipped with the GoPro camera, was unable to provide images with visible fatigue cracks. While much more economical and readily available, this UAS is not recommended for image-based fatigue crack detection.

The research team also investigated the feasibility of fatigue crack detection using passive and active thermography and two thermal cameras. Table 17 contains a summary of the passive and active infrared thermography experiments investigating fatigue crack detection.

Table 17. Summary of Infrared Thermographic Inspection Experiments

Experiment ID	Active or Passive	Specimen ID	Thermal Camera	Distance, cm (in.)	Detection (Y/N)
E015	Passive	S04	FLIR SC 640	75 (30)	N
E016	Passive	S05	FLIR SC 640	75 (30)	N
E017	Passive	S04	FLIR E8	75 (30)	Not Conclusive
E018	Passive	S05	FLIR E8	75 (30)	Not Conclusive
E019	Active	S04	FLIR E8	5 (2)	Y
E020	Active	S05	FLIR E8	5 (2)	Y

Even though the fatigue cracks were detectable in thermal images taken by the more sensitive camera, thermal fatigue detection using UASs is best with:

- Active thermography.
- Camera distance of 5 cm (2 in.).
- +/- 0.2°C sensitivity.

Chapter 5
UAS Bridge Inspection in Ashton, Idaho

Introduction

This section of the report presents the findings of a bridge inspection using UAS technology for fatigue crack detection. The bridge, located in Ashton, Idaho, carries Ashton-Flagg Ranch road traffic over the Fall River (ITD Bridge Key 21105). Figure 43 shows an aerial image of the bridge, captured by a 3DR solo UAS. The 3DR Solo is a personal UAS owned by an AggieAir pilot and was used to provide aerial and perspective images of the bridge after the under-bridge inspection was carried out with the DJI Mavic.[30] The goal of the inspection was to investigate the feasibility of using UASs for fatigue crack detection.

Figure 43. Aerial Image Captured by 3DR Solo (Courtesy of Dan Robinson)

The inspection took place on March 22, 2017, beginning at 11:30 am. According to the nearest weather station to the inspection site, KIDASHO8, which is 35 km (22 mi) away, the temperature was 10°C (50°F), Figure 44. Maximum wind speed was 25 Km/h (15 mph). However, wind gust data was not available under the bridge. Up to 40 kmh (25 mph) gusts were experienced locally (estimated by pilot and inspector) due to river channel and bridge geometry. Figure 45 and Figure 46 present the wind direction, wind speed and gust information of the inspection day, respectively, from the same weather station. Interestingly, windspeed increased just as the inspection started. The inspection lasted until 4 pm, with approximately 90 minutes of flight time, while the inspection team was standing on the Eastern bank of the river (the ground station is shown in Figure 43).

The bridge consisted of two main longitudinal frames on the Northern and Southern sides (West-East orientation), braced by 15 perpendicular transverse floor beams. Figure 47 shows one of the bridge frames on the North side. The floor beams were connected to the girder webs through gusset plates. The gusset plates of each beam were welded to the web of the main frame on each side, as seen in Figure 48. Because of the structural system, this bridge is considered a fracture critical system.

Because of the presence of fatigue cracks, the bridge is on a 12-month inspection cycle, but the cracking is not in the primary frame members. According to the inspection report, the total steel cracking in the floor beams is 3 m (10 ft) in length, in Condition State 3, and is in floor beams 4, 5, 6, 10, 11 and 12. During UBIT inspections, the inspectors found numerous hairline cracks in welds at the floor beam connections. However, no cracks have propagated into the girder webs. Magnetic particle testing verified the crack sites during the 2006 UBIT inspection with no new sites found during the 2008, 2010, 2012, 2014, 2015, or 2016 inspections. The NBI superstructure condition rating is 5. The susceptible region for fatigue crack initiation and growth was the top portion of the welded connection between the girder's web and floor beam. Figure 48 shows one of these regions. Inspectors observed fatigue cracks in susceptible regions in the previous manned inspections.
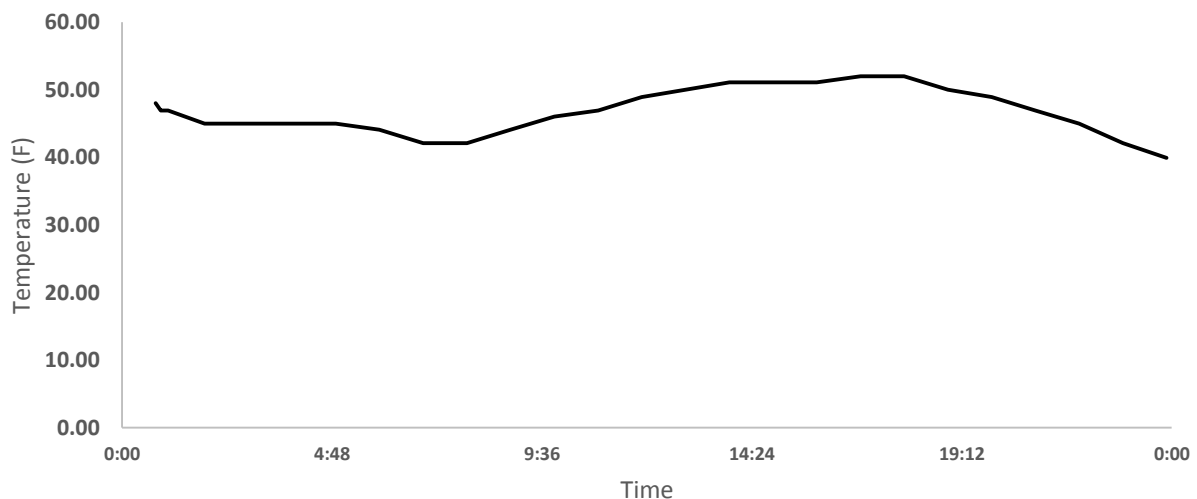
Figure 44. Daily Temperature from March 22, 2017 in Ashton from KIDASHO8 Station [31]
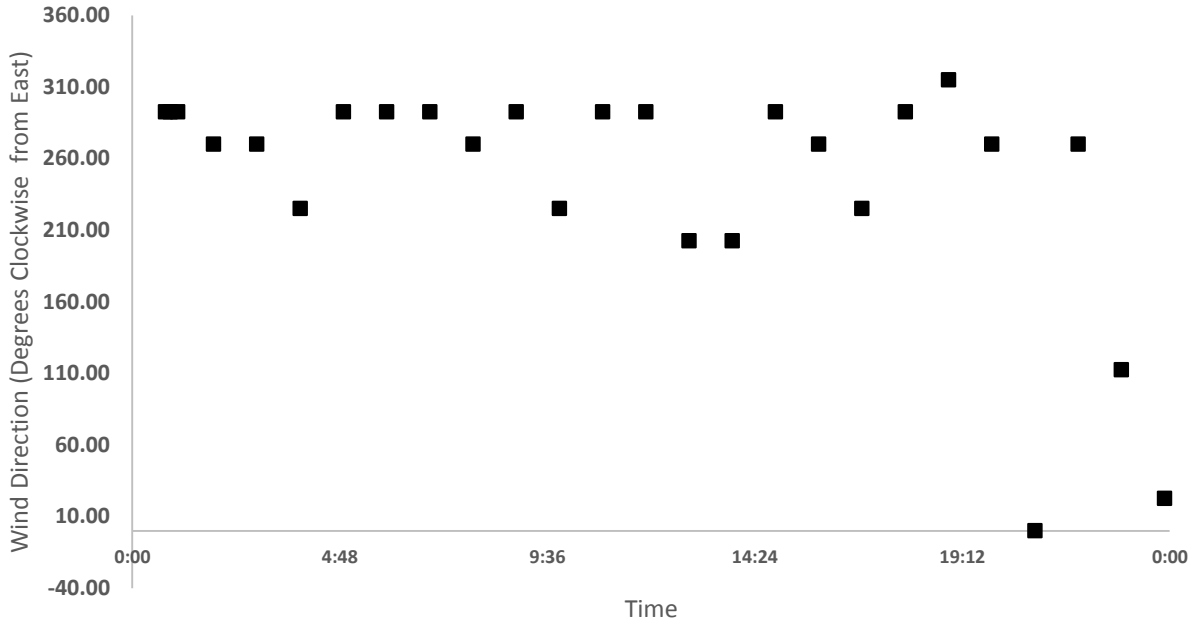
Figure 45. Wind Direction Information from March 22, 2017 in Ashton from KIDASHO8 Station[31]
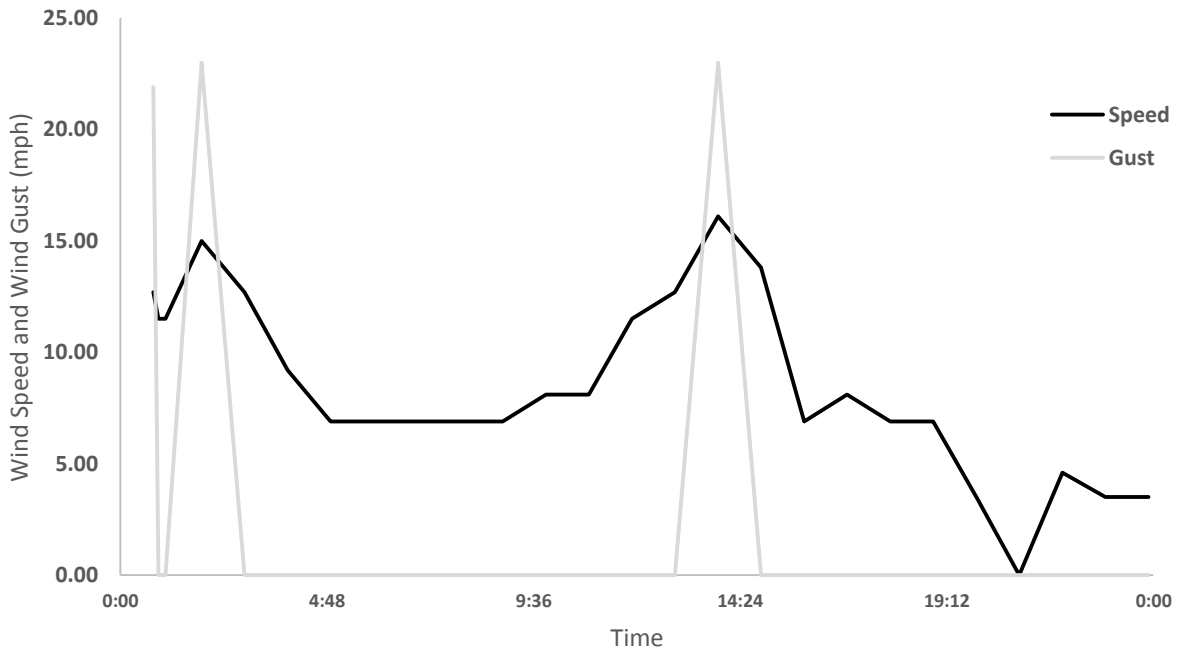
Figure 46. Wind Speed and Gust Information from March 22, 2017 in Ashton from KIDASHO8 Station[31]

Figure 47. Northern Girder of the Fall River Bridge.

Figure 48. Floor Beam Connection to Main Girder.

The research team used the DJI Mavic for the inspection. The built-in sonar sensors installed on the bottom of the UAS gave the pilot substantial control in absence of GPS signals. However, when the UAS

was flown over the river it tended to follow the river current, causing considerable instability. This is a known limitation for UAS mounted sonar. For this reason, the research team only inspected the first four Eastern floor beams and no over water inspections were carried out. The pilot flew the UAS under the bridge, inspecting 12 locations on the floor beams, two girder splices, the Southern girder web, the Southern concrete barrier, the bottom flange connection to the web on the Southern girder, and the bottom flange of the Southern girder. Figure 49 shows the UAS flying under the bridge and approaching a fatigue crack susceptible location. A handheld spotlight (Stanley FatmaxSL10LEDSL, light emitting diode, 750 lumens) held by the inspector, served a dual purpose: as a pointer to guide the pilot to the locations of interest and to provide illumination. The minimum achievable camera distance was roughly 50 cm (20 in.). However, due to the wind turbulence under the bridge, the pilot kept a distance of 75 cm (30 in.) for most of the inspection.

Figure 49. UAS Flying Under the Bridge.

Inspection Images

The inspection images were taken at different locations of the bridge: floor beams, girder splice plates, girder bottom flange web, concrete barrier, girder bottom flange, girder web, etc (E021 through E036). The total number of pictures taken by the DJI Mavic was 162. For brevity, only a handful are presented and discussed in this report, but all are available through the drop box link presented in the introduction.

Figure 50 shows schematic inspection locations. Each location has an experiment ID corresponding to the Figure 45 locations. The four floor beams from the East in the location of connections to the girders were inspected using the DJI Mavic. The main goal was to capture close-up images from the plate weld to the frame's web at both ends of these beams. ITD previously performed physical inspections in which they located two fatigue cracks on the fourth-floor beam. These cracks were marked by previous inspectors along or over the length using a black marker, with tick marks at the crack ends.
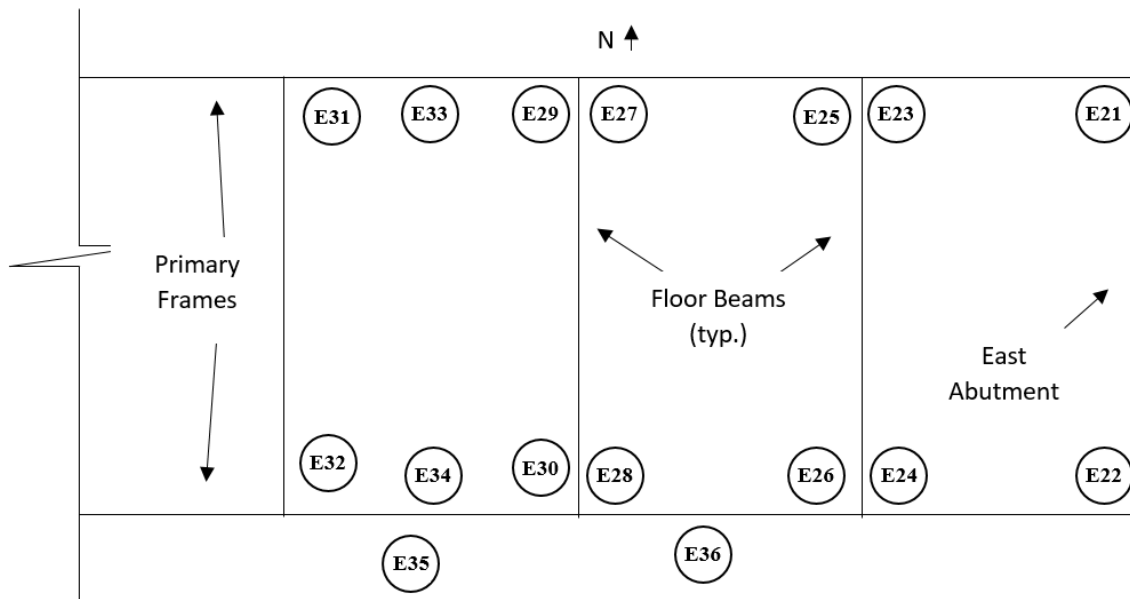
Figure 50. Plan View Drawing of the Bridge and Experiment Numbers of Inspection Locations.

Figure 51 shows the DJI Mavic image from the first floor beam (E021). The research team did not identify a fatigue crack in this image during the FPV inspection or in post-processing. Condition of the paint, minor surface corrosion, and qualitative assessment of the structural members are among the information that may be useful for the inspector. The picture from the Southern corner of this floor beam presented no detectable fatigue cracks as seen in

Figure 52 (E022). The weld in this image is covered with debris (spider sacks or webbing) which conceal the possible fatigue crack.

Tilting the camera gimbal, the UAS was able to capture images from the girder's bottom flange, web, and gusset plate weld connections to the floor beams (E023). Figure 53 is one of these images taken from the location of the second floor beam (Southern side connection). As seen in the image, no surface defect was visible. The inspection images taken from the second floor beam did not show any signs of fatigue cracking, however, the UAS detected minor deck spalling on the top of the girder on the Southern corner as shown in Figure 54. Debris covered the probable location of fatigue crack and made detection impossible (E024). The inspection images on the third floor beam were similar to the second. Figure 55 shows the surface rust on the top flange of the Northern girder (E027).

The weld connection of the fourth floor beam had two fatigue cracks, marked in black, on each end. The original image from the Northern end of this beam is shown in Figure 56 (E031). The extension of the crack was marked on the weld, obscuring the crack. Figure 57 shows the same image after zooming with an indication to locations of the crack and the marker lines (E031). The presence of the marker lines prevented the research team drawing an absolute conclusion on whether or not the fatigue crack was detectable in this image, however, there does not seem to be extension of the crack past the tick mark.

Figure 51. First Floor Beam on East, Northern Corner, No Noticeable Crack, E021

Figure 52. First Floor Beam on East, Southern Corner, Debris on the Weld, E022

Figure 53. No Cracks on Second Floor Beam on East, Southern Corner, E023

Figure 54. No Cracks on Second Floor Beam on East, Southern Corner, Minor Deck Spalling, E024

Figure 55. Third Floor Beam on East, Mild Rust, Northern Corner, E027

Figure 56. Defect (Crack) on the Fourth Floor Beam, E031
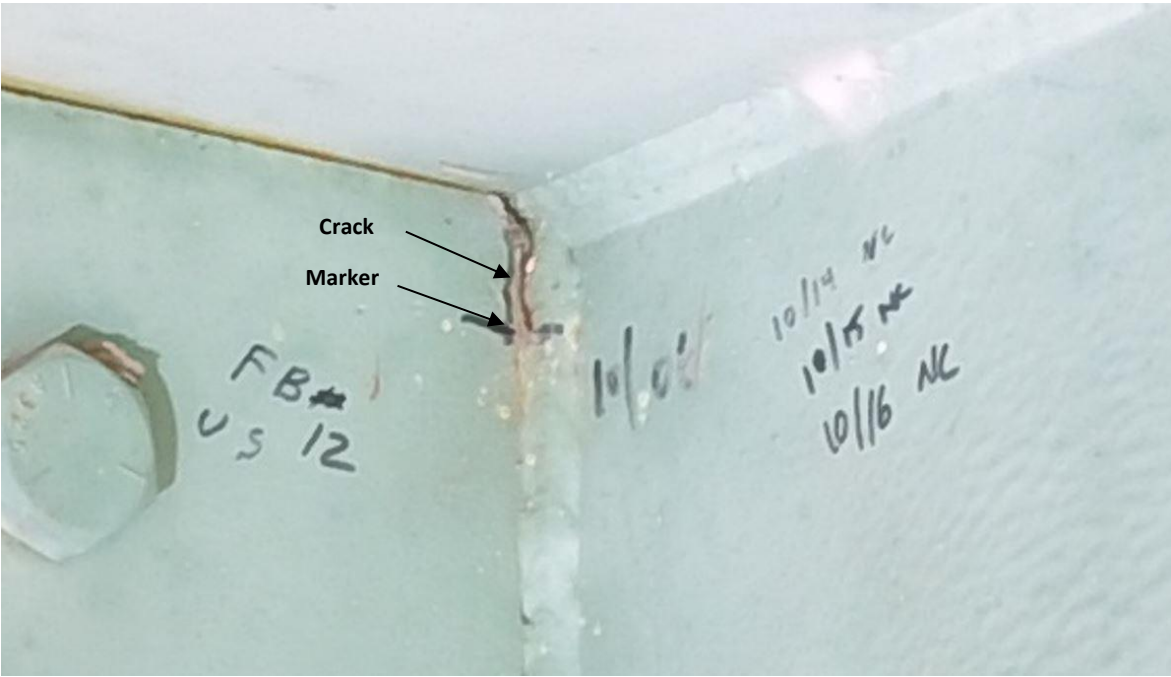
Figure 57. Zoomed Image From the Fatigue Crack, E031

On the Southern corner, the fatigue crack was seemingly shorter than the fatigue crack on the Northern corner of the fourth floor beam, according the marker lines, as shown in Figure 58. Similar to the Northern end, ITD inspectors already marked the location of the fatigue crack, and no fatigue crack is visible (E032). It does seem that ITD did not mark the length of the crack the same way as the other, but no crack is detectable prior to the tick marks. This indicates that the UAS was not close enough or photos were not of sufficient quality to find the crack. Figure 59 shows the zoomed image from the location of the fatigue crack (E032).

The research team inspected gusset plate connections to the web of girders using the UAS, and several images were taken of them (E032). No signs of fatigue cracks were found in these (see Figure 60).

The research team inspected two splice plates (E033 and E034), one on each girder, using the UAS. The UAS scanned the plates from the top to the bottom of the splices for defects. Figure 61 shows minor corrosion on the top flange splice on the Northern girder. The splice plate was in a good shape and the captured images showed no indication of defect (E033).

The web splice plate and the nuts on the Southern side girder had minor surface rust as shown in Figure 62 (E034). The rest of the plate was seemed to be sound.

Inspection images from the bottom of the Southern concrete deck overhang and the barrier showed possible delamination and efflorescence (E035), as shown in Figure 63. The UAS captured a side view of the girder, as seen in Figure 64, which shows cracks and possible delamination (E036).

Finally, the UAS scanned the bottom flange of the Southern girder. Except for mild surface corrosion, the bottom flange was in a sound condition, as seen in Figure 65. The concrete deck efflorescence was visible as well on the right side of this image (E035 and E036).

Image Processing and the Inspection Images

The research team applied image processing techniques on the images for autonomous defect (fatigue crack) detection (E037). However, the fatigue cracks were not explicitly visible in the inspection images before image processing. For crack detection in this dataset, the research team applied the customized LoG filter developed in Chapter 4 to the inspection images. Figure 66 shows the superimposed detected edges on the original image. The algorithm detected the full length of the marker lines along with the edges of the structural members. The superfluous edges could be removed with additional filtering effort. The presence of marker lines interfered with the program performance in crack detection. Therefore, no certain conclusions regarding the program's fatigue crack detection capabilities can be made.

Figure 67 shows the results of the proposed image processing technique on an image without fatigue cracks. Since there were no cracks and therefore no marker lines, no detection was reported on the susceptible region. The members' edges were detected by the program.

UAS Fatigue Crack Detection Comparison to Manned Inspections

The research team was unable to detect fatigue cracks in the inspection images; therefore, an actual comparison cannot be performed. However, the marker lines were clearly visible in the images of fatigue cracks. The inspection results cannot be used to draw a solid conclusion about the ability of UASs for fatigue crack detection.

Figure 58. Defect (Crack) on the Fourth Floor Beam, Southern Corner, E032

Figure 59. Zoomed Image from the Fatigue Crack on the Fourth Floor Beam, Southern Corner, E032

Figure 60. No Defects (Crack) on the Fourth Floor Beam, Southern Corner, Bottom Flange Weld, E032

71

Figure 61. Minor Corrosion on Top of the Northern Girder Splice (First Splice from East), E033
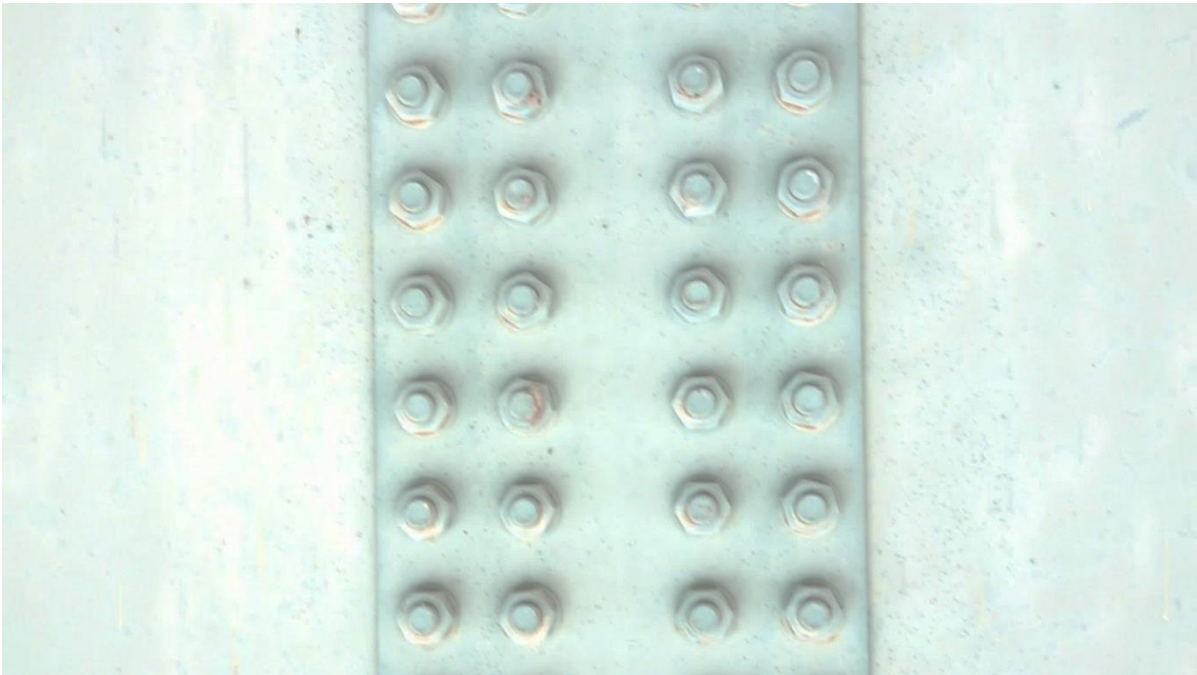
Figure 62. Minor Corrosion on the Plate and Nuts, Southern Girder Splice (First Splice from East), E034
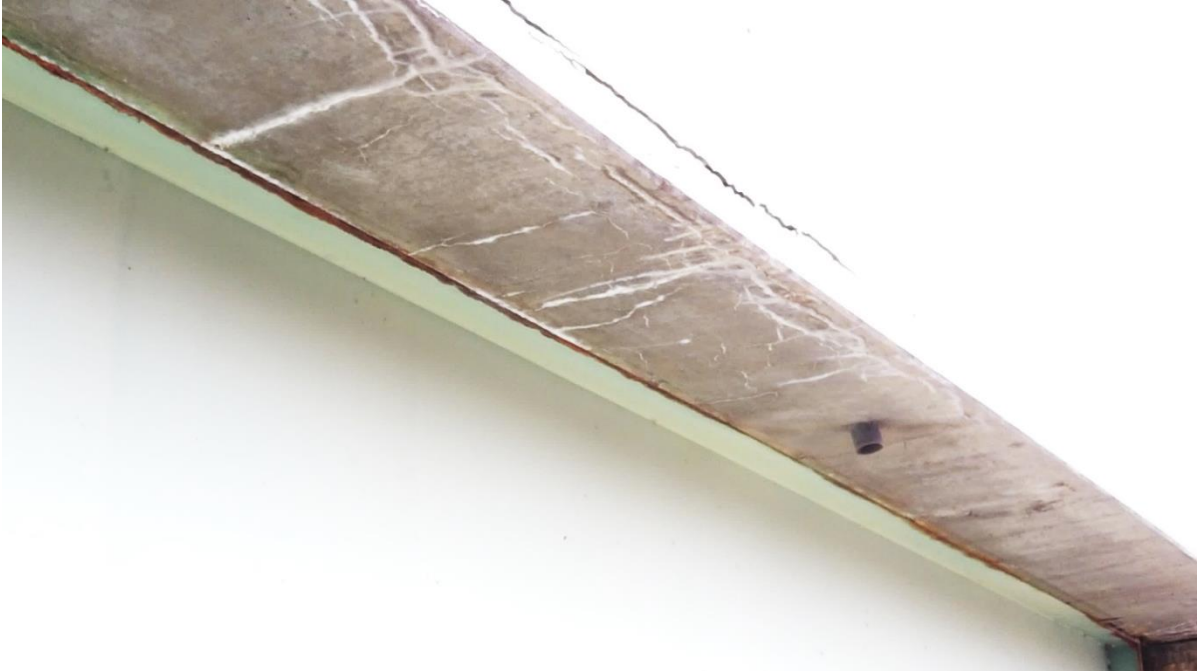
Figure 63. Cracks, Possible Delamination, and Efflorescence on the Southern Bearing, E035

Figure 64. Cracks and Possible Delamination on the Southern Barrier, E036

Figure 65. Minor Corrosion on Bottom Flange of the Southern Girder, E035 and E036
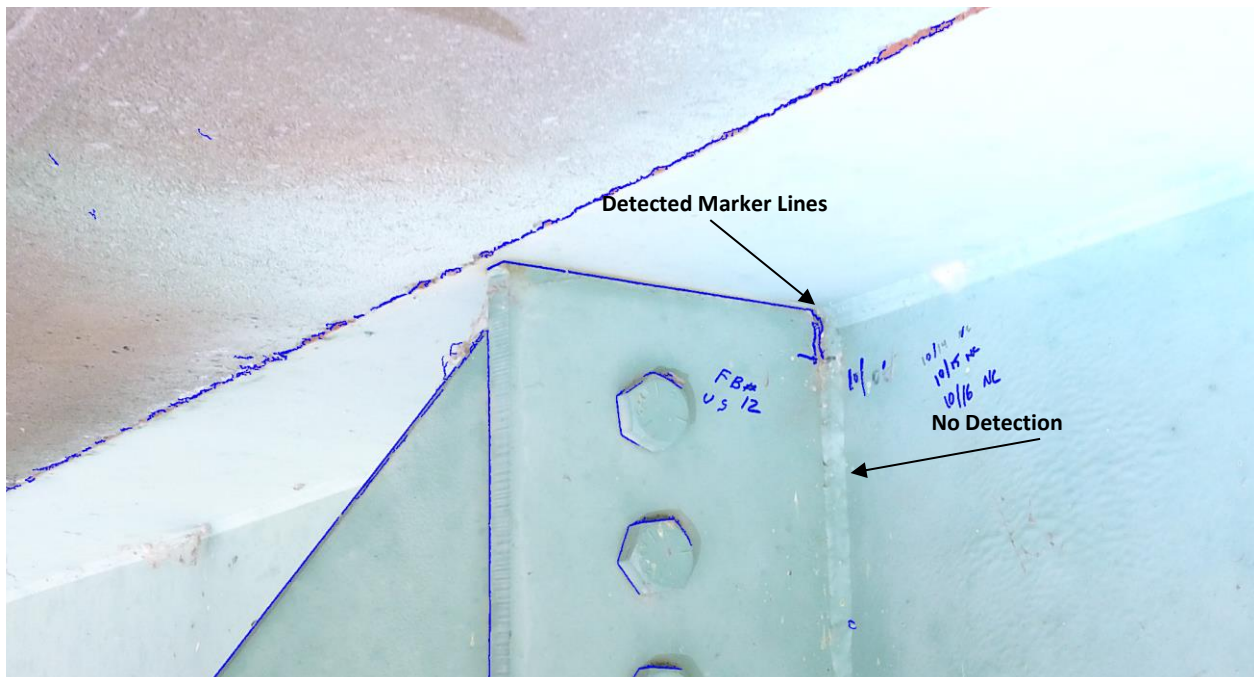
Figure 66. Image Processing on Captured Image with Crack, E037
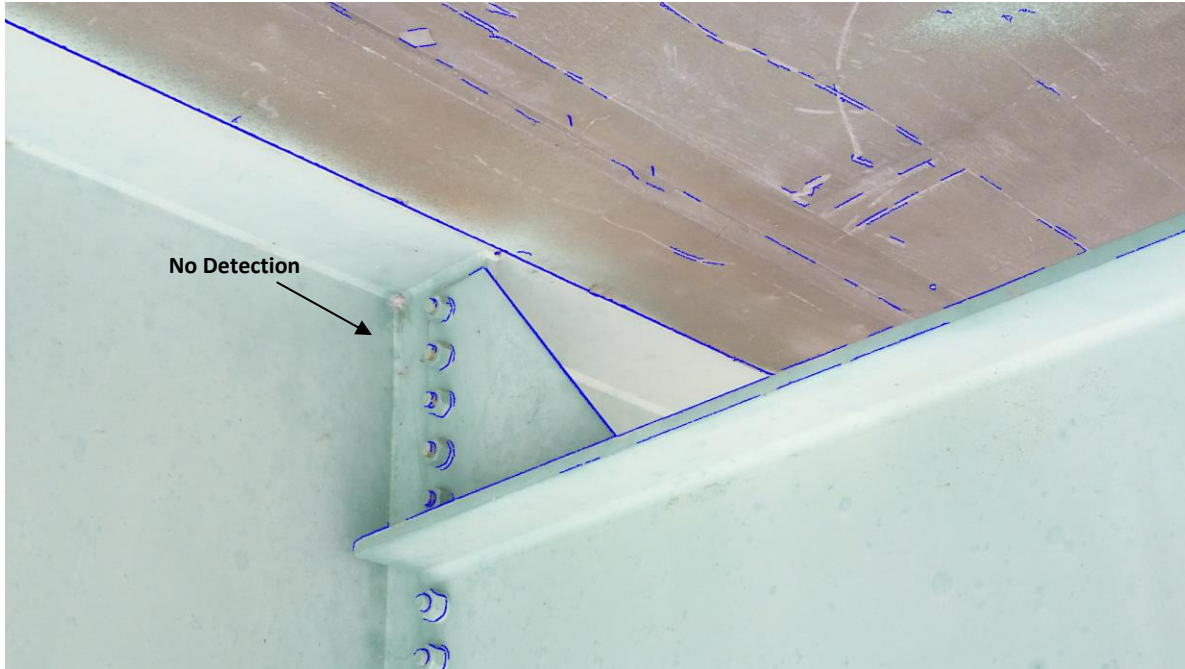
Figure 67. Image Processing on Captured Image without Crack, E037

Conclusions from the Fall River Bridge Inspection

The research team inspected an in-service bridge in Ashton, Idaho using a DJI Mavic UAS. The main goal of the inspection was to detect existing fatigue cracks. Twelve locations on the floor beams, two splice plates, one concrete barrier, one girder web, and one girder bottom flange were among the locations the UAS covered in this inspection.

Reviewing the UAS images, the research team concluded the following:

- UAS images capture concrete cracks, delamination, efflorescence, minor surface rusting, and poor paint conditions (E033 through E036).
- Known fatigue cracks were not visible in captured images (E031 and E032).
- Marks, drawn lines, spider webs, water stains, and unknown debris will hinder the detection of fatigue cracks using only visual images (E031 and E032).
- Fatigue crack detection success is limited by camera capability and how close the UAS can get to the inspection location in the underbridge environment.
- The UAS fatigue crack detection on the in-service bridge was unsuccessful.

Reviewing the flight performance, the research team concluded:

- Wind speeds of 25 Km/h (15 mph) with gust speed of 40 kmh (25 mph) played a significant role in achieving the desired camera distance.

- Inspection of all floor beams by UAS was not possible since the UAS could not be controlled over the water flowing in the river (downward sonar sensor limitation).
  - Many UASs use this feature, which should be considered in future UAS inspections over water. With most UAS, this feature can be turned off, but performance will either further deteriorate or be ineffective.
  - Other GPS-denied avionic sensors should be investigated and evaluated for aiding under-bridge UAS control. Potential sensors include, LiDAR, upward mounted sonar or laser range finders, additional on-board barometers, and additional image based navigational sensors. Sensors pointed upward at the bridge deck rather than downward where water is likely present are likely to have success.

Chapter 6
Conclusions

Conclusions

Many types of bridge inspections are time consuming, expensive, dangerous, and tedious. Because of this, much research has been focused on finding alternatives or better protocols for bridge inspections. UASs have shown promising results in previous research performed by many state DOTs. These studies have found significant limitations, but also successes. The most common UAS applications studied by DOTs were traffic monitoring and surveillance, road condition assessment, and mapping. However, in bridge inspections, UASs have shown varying degrees of success. Only a handful of DOTs have studied feasibility of bridge inspections using UASs: California, Georgia, Michigan, Minnesota, Florida, and Idaho. This study focused on using UASs for under-bridge inspections, with an emphasis on fatigue crack detection.

The following observations can be made about UAS from the *literature review*:

- The recent advances of UAS have the potential to provide low cost options to gather previously difficult or expensive images.[12,4]
- There have been mixed successes with UAS aided bridge inspections throughout the United States. Some cases have resulted in successful inspections in easily accessible locations where the UAS has access to GPS, the most reliable and effective tool for UAS autopilots.[9,4]
- UAS control options need to improve so that a pilot can safely and effectively obtain stable images of every part of a bridge in any reasonable weather, especially without the aid of GPS.[12]
- Weather currently plays too big of a role in UAS flight success, which is a very significant barrier for many state agencies with very tight inspection schedules. [4]
- Current FAA restrictions are not too burdensome for an agency to perform some inspections, but provide significant challenges. Regulations will relax over time, as in the past, as public perception, UAS reliability, and autonomous controls continue to improve.[11, 4]

The following observations and conclusions are made from the *small bridge experiment*:

- Image processing techniques (3D mapping or damage detection) that can detect defects are a significant advantage of a UAS inspection (E002 and E005), but must be tailored to the situation. Also, 3D mapping is not likely to be useful at this time without significant effort based on the experience with off-the-shelf software (E005).
- Real-time and automated visual concrete deck crack detection is possible and effective with 90 percent detection (E001 and E002).
- Light girder corrosion was detectable in real-time (E004).

- Concrete delamination detection was shown to be feasible using thermography and would provide a promising area of additional research (E003).
- Image processing techniques can be used to help the inspector find fatigue or concrete cracks and show promise for automated detection.

In this study, the research team investigated the feasibility of fatigue crack detection using two remote sensing methodologies: visual and thermal images. Three UASs were used to capture images of a fatigue crack. These images helped the research team provide crack detection requirements in terms of lighting condition and camera distance to investigate the feasibility of fatigue crack detection in GPS-denied environments in a no wind situation and to assess the UAS-based fatigue crack detection with GPS-denied navigation under a bridge.

The requirements for fatigue crack detection using three cameras (no UAS) in terms of camera distance and lighting conditions, in *highly controlled office conditions*, were determined as follows (E006 through E008):

- Only the DJI Mavic camera took pictures with recognizable cracks in all lighting conditions (E007).
- Based on the results from the Nikon and DJI Mavic camera, minimum surface illumination of 200 lx was recommended to capture proper images, even though the DJI Mavic was successful at lower lx. It is acknowledged that this may not be feasible in all situations. UAS mounted lights, or handheld spot lights, or both can be used effectively to increase surface illumination (E007 and E008).
- The furthest camera distance for an image with visible fatigue crack was achieved with the Nikon camera in the Normal condition: 30 cm (12 in.), E008.

The research team used three UAS to capture images of a test-piece with a known fatigue crack. This was done in the SMASH lab using three UAS: the 3DR Iris, equipped with a GoPro camera; the Goose, equipped with a Nikon camera; and the DJI Mavic. The images from this semi-realistic inspection were used to determine if fatigue crack detection using UASs is feasible (E009 through E011). The findings from this experiment under *GPS-denied, but environmentally controlled conditions* are outlined below:

- Crack detection in DJI Mavic images was feasible in all lighting conditions (E010). Crack detection was enhanced by the DJI Mavic's superior stability, which allowed the UAS to reach a closer camera distance to the inspected piece, and the camera's exposure adjustment for darker scenes.
- The 3DR Iris, equipped with the GoPro camera, was not stable enough to provide the required camera distance in the absence of GPS signals, and therefore was not recommended for this task (E009).

- The inspection results of the Goose, equipped with the Nikon camera, allowed the detection of the fatigue crack in the test piece. The camera distance was 70 cm (35 in.) and the camera was pre-zoomed, however the images was blurry due to vibrations (E011).

The UAS were used to *inspect the test piece underneath the UWRL Bridge* to find the fatigue crack on S001 in an uncontrolled environment (E012 and E013):

- Due to the 32 km/h (20 mph) wind, with maximum gust speed of 45 km/h (28 mph), the minimum safe camera distance for the 3DR Iris was 60 cm (24 in.), which was greater than what was achieved in the SMASH lab, 50 cm (20 in.), and there was no detection in the images (E012).
- The pilot was able to provide a similar camera distance to that in the SMASH lab experiment with the DJI Mavic, 25 cm (10 in.) in experiment E013.
- Only the DJI Mavic pictures showed the fatigue crack (E013)
- The DJI Mavic showed the fatigue crack in all lighting conditions (E013).
- The Goose was not flown due to the low clearance of the bridge.

Finding fatigue cracks using image processing techniques was feasible when the research team used the DJI Mavic to capture the images and used the LoG edge detector as the primary image processing algorithm (E014). The experiment on the UWRL bridge showed that the DJI Mavic was the best device of the three UASs to help a bridge inspector find the fatigue cracks. This UAS provides images with visible fatigue cracks, even in different lighting conditions. The 2X digital zoom and the ability to change the camera exposure enhanced the quality of the FPV real-time inspection. Also, the sonar altitude hold sensor stabilized the UAS, even during pilot described undesirable wind conditions (E012).

The Goose, as equipped, was sufficient for finding some cracks in the laboratory, but its images exhibited much blurrier pictures, which was thought to be detrimental to the inspection process. Additionally, its control hardware, software, and size made the UAS more difficult to control compared to the DJI Mavic. The advantage of the Goose as a UAS is its payload capacity and with additional tuning of its flight characteristics, the Goose may eventually be considered feasible when additional sensors are mounted on the UAS. Overall, the limitations of the Goose were such that it did not perform on the same level as the off-the-shelf DJI Mavic.

The inspection simulations in the SMASH lab and at the UWRL bridge showed that the 3DR Iris, equipped with the GoPro camera, was unable to provide images with visible fatigue cracks. While much more economical and readily available, this UAS is not recommended for image-based fatigue crack detection.

The research team also investigated the feasibility of fatigue crack detection using passive and active thermography and two thermal cameras (E015 through E020). Even though the fatigue cracks were detectable in thermal images taken by the more sensitive camera, thermal fatigue detection using UASs is best with:

- Active thermography.
- Camera distance of 5 cm (2 in.).
- +/- 0.2ºC sensitivity.

For a real inspection, an in-service bridge in Ashton, Idaho, was inspected using a DJI Mavic UAS (E021 through E037). The primary goal of the inspection was to detect existing fatigue cracks. Twelve locations on the floor beams, two splice plates, one concrete barrier, one frame web, and one frame bottom flange were among the locations covered by the UAS in this inspection.

Reviewing the UAS images from the Ashton, Idaho bridge inspection, one can conclude the following:

- UAS images capture concrete cracks, delamination, efflorescence, minor surface rusting, and poor paint conditions (E033 through E036).
- Known fatigue cracks were not visible in captured images (E031 and E032).
- Marks, drawn lines, spider webs, water stains, and unknown debris will hinder the detection of fatigue cracks using only visual images (E031 and E032).
- Fatigue crack detection success is limited by camera capability and how close the UAS could get to the inspection location in the under-bridge environment.
- The UAS fatigue crack detection on the in-service bridge was unsuccessful.

Reviewing the flight performance from the Ashton, Idaho bridge inspection, the following can be concluded:

- Wind speeds of 25 Km/h (15 mph) with gust speed of 40 Km/h (25 mph) played a significant role in achieving the desired camera distance.
- Inspection of all floor beams by UAS was not possible since the UAS could not be controlled over the water flowing in the river (downward sonar sensor limitation).
  - Many UASs use this feature, which should be considered in future UAS inspections over water. With most UAS, this feature can be turned off, but performance will either further deteriorate or be ineffective.
  - Other GPS-denied avionic sensors should be investigated and evaluated for aiding under-bridge UAS control. Potential sensors include, LiDAR, upward mounted sonar or laser range finders, additional on-board barometers, and additional image based navigational sensors. Sensors pointed upward at the bridge deck rather than downward where water is likely present are likely to have success.

Recommendations and Future Work

According to the results of this study, the following recommendations regarding use of UASs for under-bridge inspection and fatigue crack detection are made:

- Using UASs with autopilot controls such as sonar, LiDAR, visual sensors, or obstacle avoidance is a necessity under a bridge when GPS-denied.
- Downward mounted sonar is not effective overwater (like with the DJI Mavic) and other sensors may have similar issues. Future UAS should be tested prior to implementation.
- The geometry of probable fatigue crack locations makes obtaining the required camera distance for fatigue crack detection difficult, especially in windy conditions.
- It is recommended that some minimal optical zoom is considered for future use to compensate for the camera distance issues. Too much optical zoom amplifies UAS vibrations and can compromise the images.
- Some UAS cameras, not those in this study, can be outfitted with high power lenses which effectively pre-zoom the camera. These lenses could be a promising option for fatigue crack detection.
- Ideal flying conditions are not always possible and inspections cannot always be delayed, making the wind speed limitations of UASs a significant drawback. Flying in wind speed of 40 km/h (25 mph) or more to find fine defects is not recommended, even with autopilot features and GPS enabled.

The following are recommendations for future work in the area of UAS under-bridge inspections:

- Fatigue crack detection using thermography is promising, however, a thermal camera with a sensitivity of +/- 0.2°C or better is recommended but this topic requires further study.
- There was indication that vibration affected the results of the thermal images, indicating an additional study should be performed to determine if this significantly affects images.
- Large defects like concrete cracks, efflorescence, paint condition etc., are likely still detectable in windy conditions, even in a GPS-denied environment. A robust analysis including multiple professional inspectors and pilots for a quantitative inspection comparison should be performed on all defect types to assess UAS inspection probability of detection.

References

1. Idaho Transportation Department, Idaho Manual for Bridge Evaluation, 2016 Edition, Boise, ID. http://apps.itd.idaho.gov/apps/Bridge/manual/IMBE2016.pdf.

2. Air Mobility Command. "Aeronautical Information Manual: Official Guide to Basic Flight Information and ATC Procedures" (February 9, 2012)

3. Fact Sheet – Small Unmanned Aircraft Regulations (Part 107) "Fact Sheet – Small Unmanned Aircraft Regulations (Part 107)". 2017. *Faa.Gov*. Accessed April 10 2017. https://www.faa.gov/news/fact_sheets/news_story.cfm?newsId=20516.

4. Otero, Luis Daniel, N. Gagliardo, D. Dalli, W. H. Huang, and P. Cosentino. "Proof of Concept for Using Unmanned Aerial Vehicles for High Mast Pole and Bridge Inspections." *Contract BDV28* (2015): 977-02.

5. "FAA Issues Part 107 Waivers, Airspace Authorizations". Upated April 2016. *Faa.Gov*. Accessed April 10 2017. https://www.faa.gov/news/updates/?newsId=86707.

6. "Certificates of Waiver or Authorization (COA)". 2017. *Faa.Gov*. Accessed April 10 2017. https://www.faa.gov/about/office_org/headquarters_offices/ato/service_units/systemops/aaim/organizations/uas/coa/.

7. Pajares, Gonzalo. "Overview and Current Status of Remote Sensing Applications Based on Unmanned Aerial Vehicles (UASs)." *Photogrammetric Engineering & Remote Sensing* 81, no. 4 (2015): 281-329.

8. Bento, Maria D., *Unmanned Aerial Vehicles: An overview*, InsideGNSS, January 2008. www.insidegnss.com/auto/janfeb08-wp.pdf.

9. Moller, Paul S. "CALTRANS Bridge Inspection Aerial Robot." *Final Report, CA* 8 (2008): 0182.

10. Irizarry, Javier, and Eric N. Johnson. *Feasibility Study to Determine the Economic and Operational Benefits of Utilizing Unmanned Aerial Vehicles (UASs)*. Georgia Institute of Technology, 2014.

11. Brooks, Colin, Richard J. Dobson, David M. Banach, David Dean, Thomas Oommen, Rudiger Escobar Wolf, Timothy C. Havens, Theresa M. Ahlborn, and Ben Hart. *Evaluating the Use of Unmanned Aerial Vehicles for Transportation Purposes*. No. RC-1616. Michigan Tech Research Institute, Ann Arbor, Michigan, 2015.

12. Zink, Jennifer, and Barritt Lovelace. *Unmanned Aerial Vehicle Bridge Inspection Demonstration Project*. No. MN/RC 2015-40. 2015.

13. Farradine, P.B., 2005. *Use of Unmanned Aerial Vehicles in Traffic Surveillance and Traffic Management*. Technical Memorandum Prepared for: Florida Department of Transportation.

14. AASHTO Survey Fact Sheet (2016), https://indd.adobe.com/view/78d3b1d3-13c3-42c0-8bf2-75ea8c534d1a.

15. Dorafshan S., Maguire, M., and Chang, M., (2017). Comparing Automated Image-Based Crack Detection Techniques in Spatial and Frequency Domains, 26th ASNT Research Symposium, Jacksonville, Florida.

16. Talab, Ahmed Mahgoub Ahmed, Zhangcan Huang, Fan Xi, and Liu HaiMing. "Detection crack in image using Otsu method and multiple filtering in image processing techniques." *Optik-International Journal for Light and Electron Optics* 127, no. 3 (2016): 1030-1033.

17. Dorafshan, Sattar, Marc Maguire, and Xiaojun Qi. "Automatic Surface Crack Detection in Concrete Structures Using OTSU Thresholding and Morphological Operations." Report to the Utah Transportation Center, Utah State University, 2016.

18. Abdel-Qader, I., Abudayyeh, O., & Kelly, M. E. (2003). Analysis of edge-detection techniques for crack identification in bridges. *Journal of Computing in Civil Engineering*, *17*(4), 255-263.

19. Hutchinson, T. C., & Chen, Z. (2006). Improved image analysis for evaluating concrete damage. *Journal of Computing in Civil Engineering*, *20*(3), 210-216.

20. Nishikawa, T., Yoshida, J., Sugiyama, T., & Fujino, Y. (2012). Concrete crack detection by multiple sequential image filtering. *Computer-Aided Civil and Infrastructure Engineering*, *27*(1), 29-47.

21. "Agisoft Photoscan". 2017. *Agisoft.Com*. Accessed April 11 2017. http://www.agisoft.com/.

22. Dexter, R. J., & Ocel, J. M. (2013). *Manual for repair and retrofit of fatigue cracks in steel bridges* (No. FHWA-IF-13-020). https://trid.trb.org/view.aspx?id=1308583.

23. Lee, Sangwook, and Nikolas Kalos. "Bridge Inspection Practices Using Non-destructive Testing Methods." *Journal of Civil Engineering and Management* 21, no. 5 (2015): 654-665.

24. Thompson, Donald O., and Dale E. Chimenti, eds. *Review of progress in quantitative nondestructive evaluation*. Vol. 18. Springer Science & Business Media, 2012.

25. DelGrande, Nancy, and Philip F. Durbin. "Delamination detection in reinforced concrete using thermal inertia." In *Nondestructive Evaluation Techniques for Aging Infrastructures & Manufacturing*, pp. 186-197. International Society for Optics and Photonics, 1999.

26. Incropera, Frank P., and David P. De Witt. "Fundamentals of heat and mass transfer." (1985).

27. Negar, N., Williams, D., Schwartz, J., Ahamed, S. I., & Smith, R. O. (2014, June). Smartphone-based Light Intensity Calculation Application for Accessibility Measurement. In *Proceedings of the RESNA Annual Conference, Indianapolis, IN, USA* (pp. 11-15).

28. "Weather History For Logan, UT | Weather Underground". 2017. *Wunderground.Com*. https://www.wunderground.com/history/airport/KLGU/2017/1/10/DailyHistory.html?req_city=Logan&req_state=UT&req_statename=&reqdb.zip=84321&reqdb.magic=1&reqdb.wmo=99999

29. FLIR Systems, Inc. 2017. "FLIR Thermacam Researcher Software - FLIR Thermal Imaging". *Flir.Co.Uk*. Accessed April 12 2017. http://www.flir.co.uk/cs/display/?id=42404.

30. "Aggieair | A Remote Sensing Unmanned Aerial System For Scientific Applications". 2017. *Aggieair.Usu.Edu*. Accessed April 12 2017. http://aggieair.usu.edu/.

31. "Weather History For Ashton, ID | Weather Underground". 2017. *Wunderground.Com*. https://www.wunderground.com/personal-weather-station/dashboard?ID=KIDASHTO8#history/s20170322/e20170322/mdaily

Appendix A
List of Specimens and Experiments

Table 18. Schedule of Specimens

Specimen ID	Source	Defect	Form	Dimensions
S01	USU	Surface Concrete Cracks	Lab-made Bridge deck	20' x 13' x 0.75'
S02	USU	Surface Corrosion	Steel Girder 1	W10 x 88
S03	USU	Deck Delamination	Lab-made Bridge deck	20' x 13' x 0.75'
S04	ITD	Fatigue Crack	Steel Puck 1	D= 1.65" (4.2 cm)
S05	ITD	Fatigue Crack	Steel Puck 2	D = 1.6 5" (4.2 cm)
S06	ITD	Possible Fatigue Crack	Floor Beam to Girder Connection	N/A
S07	ITD	Possible Fatigue Crack	Floor Beam to Girder Connection	N/A
S08	ITD	Possible Fatigue Crack	Floor Beam to Girder Connection	N/A
S09	ITD	Possible Fatigue Crack	Floor Beam to Girder Connection	N/A
S10	ITD	Possible Fatigue Crack	Floor Beam to Girder Connection	N/A
S11	ITD	Possible Fatigue Crack	Floor Beam to Girder Connection	N/A
S12	ITD	Possible Fatigue Crack	Floor Beam to Girder Connection	N/A
S13	ITD	Possible Fatigue Crack	Floor Beam to Girder Connection	N/A
S14	ITD	Possible Fatigue Crack	Floor Beam to Girder Connection	N/A
S15	ITD	Possible Fatigue Crack	Floor Beam to Girder Connection	N/A
S16	ITD	Fatigue Crack	Floor Beam to Girder Connection	N/A
S17	ITD	Fatigue Crack	Floor Beam to Girder Connection	N/A
S18	ITD	Surface Corrosion	Girder Splice	N/A
S19	ITD	Surface Corrosion	Nuts	N/A
S20	ITD	Efflorescence and Cracks	Concrete Barrier	N/A
S21	ITD	Delamination and Cracks	Concrete Barrier	N/A

Table 19. List of Experiments

Experiment ID	Subfolders	Intent	Specimen	UAS	Camera	Site	Page in the Report
E001	None	Detect Concrete Cracks (Manually)	S01	3DR Iris	GoPro Hero 4	SMASH Lab	16-17
E002	None	Detect Concrete Cracks (Autonomously)	S01	3DR Iris	GoPro Hero 4	SMASH Lab	17-18
E003	None	Detect Concrete Delamination	S03	N/A	FLIR E8 Thermal Camera	SMASH Lab	19-20
E004	None	Detect Steel And Weld Corrosion	S02	3DR Iris	GoPro Hero 4	SMASH Lab	20-21
E005	E5-1 / E5-2	3D Model Construction	S01	3DR Iris	GoPro Hero 4	SMASH Lab	21-22
E006	None	Detect Fatigue Crack (Minimum Requirements)	S04	3DR Iris[*]	GoPro Hero 4	Indoors (Office)	27-28
E007	None	Detect Fatigue Crack (Minimum Requirements)	S04	DJI Mavic[*]	DJI Built-In	Indoors (Office)	30, 33
E008	None	Detect Fatigue Crack (Minimum Requirements)	S04	Goose[*]	Nikon Camera	Indoors (Office)	30, 34
E009	None	Detect Fatigue Crack (Visual Inspection)	S04	3DR Iris	GoPro Hero 4	Indoors (SMASH Lab)	35, 37
E010	None	Detect Fatigue Crack (Visual Inspection)	S04	DJI Mavic	DJI Built-In	Indoors (SMASH Lab)	35, 38, 39
E011	None	Detect Fatigue Crack (Visual Inspection)	S04	Goose	Nikon Camera	Indoors (SMASH Lab)	35, 40
E012	None	Detect Fatigue Crack (Visual Inspection)	S04	3DR Iris	GoPro Hero 4	Outdoors (UWRL)	42-45
E013	None	Detect Fatigue Crack (Visual Inspection)	S04	DJI Mavic	DJI Built-In	Outdoors (UWRL)	44, 46-49
E014	None	Detect Fatigue Crack (Autonomously)	S04 S05	DJI Mavic	DJI Built-In	N/A	51-53
E015	None	Detect Fatigue Crack (Passive	S04	N/A	FLIR SC 640	Indoors (Office)	54-55

		Thermography)				
E016	None	Detect Fatigue Crack (Passive Thermography)	S05	N/A	FLIR SC 640	Indoors (Office)	54, 56
E017	None	Detect Fatigue Crack (Passive Thermography)	S04	N/A	FLIR E8	Indoors (Office)	56-57
E018	None	Detect Fatigue Crack (Passive Thermography)	S05	N/A	FLIR E8	Indoors (Office)	57-58
E019	None	Detect Fatigue Crack (Active Thermography)	S04	N/A	FLIR E8	Indoors (Office)	58, 60
E020	None	Detect Fatigue Crack (Active Thermography)	S05	N/A	FLIR E8	Indoors (Office)	50, 61, 62
E021	None	Detect Possible Fatigue Crack (Visually in Ashton)	S06	DJI Mavic	DJI Built-In	Outdoors (Ashton, ID)	75-77
E022	None	Detect Possible Fatigue Crack (Visually in Ashton)	S07	DJI Mavic	DJI Built-In	Outdoors (Ashton, ID)	75-77
E023	None	Detect Possible Fatigue Crack (Visually in Ashton)	S08	DJI Mavic	DJI Built-In	Outdoors (Ashton, ID)	75,76, 78
E024	None	Detect Possible Fatigue Crack (Visually in Ashton)	S09	DJI Mavic	DJI Built-In	Outdoors (Ashton, ID)	75, 76, 78
E025	None	Detect Possible Fatigue Crack (Visually in Ashton)	S10	DJI Mavic	DJI Built-In	Outdoors (Ashton, ID)	75
E026	None	Detect Possible Fatigue Crack (Visually in Ashton)	S11	DJI Mavic	DJI Built-In	Outdoors (Ashton, ID)	75
E027	None	Detect Possible Fatigue Crack (Visually in Ashton)	S12	DJI Mavic	DJI Built-In	Outdoors (Ashton, ID)	75, 76, 79
E028	None	Detect Possible Fatigue Crack (Visually in Ashton)	S13	DJI Mavic	DJI Built-In	Outdoors (Ashton, ID)	75
E029	None	Detect Possible Fatigue Crack (Visually in Ashton)	S14	DJI Mavic	DJI Built-In	Outdoors (Ashton, ID)	75

E030	None	Detect Possible Fatigue Crack (Visually in Ashton)	S15	DJI Mavic	DJI Built-In	Outdoors (Ashton, ID)	75
E031	None	Detect Known Fatigue Crack (Visually in Ashton)	S16	DJI Mavic	DJI Built-In	Outdoors (Ashton, ID)	75, 76, 79, 80
E032	None	Detect Known Fatigue Crack (Visually in Ashton)	S17	DJI Mavic	DJI Built-In	Outdoors (Ashton, ID)	75, 80, 82, 83
E033	None	Detect Surface Corrosion	S18	DJI Mavic	DJI Built-In	Outdoors (Ashton, ID)	75, 80, 83
E034	None	Detect Surface Corrosion	S19	DJI Mavic	DJI Built-In	Outdoors (Ashton, ID)	75, 80, 84
E035	None	Detect Efflorescence and Cracks	S20	DJI Mavic	DJI Built-In	Outdoors (Ashton, ID)	75, 81, 84
E036	None	Detect Delamination and Cracks	S21	DJI Mavic	DJI Built-In	Outdoors (Ashton, ID)	81, 85
E037	None	Detect Fatigue Cracks (Autonomously)	S22	DJI Mavic	DJI Built-In	Outdoors (Ashton, ID)	86, 87

[*]Static UAS without flying

Appendix B
Concrete Crack Detection Code

```
clc
clear
close all
file=dir('C:\NDS\*.jpg');
NF=length(file);
orImage=cell(NF,1);
grayIm=cell(NF,1);
MedianIm=cell(NF,1);
edge=cell(NF,1);
binaryIm=cell(NF,7);
% Creating a cell array for each binary image during each stage of the code,
% '1' binary image constructed from applying Otsu's thresholding method
% '2' binary image constructed from applying area cutoff value of 200
% '3' binary image constructed from applying orientation cutoff value to
% ramove vertical and horizontal lines
% '4' binary image constructed from applying morphological operation of
% majority
% '5' binary image constructed from applying morphological operation of
% bwareaopen to connect objects
% '6' binary image constructed from applying another threshold on S
% component of the HSV of original image to reduce the non-concrete
% background
% '7' binary image to show the skleton of the cracks
RecIm=cell(NF,1);
% Cell array to save the reconstructed image
Cracks_L=cell(NF,1);
% Cell array to save length of cracks detected in final step
Hx=[-1 -2 -1;0 0 0;1 2 1];
% Sobel filter to detect Horizontal lines
Hy=Hx';
% Sobel filter to detect Vertical lines
paper_ap=cell(NF,7);
```

```
% Define cell array to save resultant images using paper approach
paper_cracksL=zeros(NF,1);
% Vector to save length of cracks detected in final step
position=[50,50];
% Define the position of the label
for i=1:1
   orImage{i}=imread('back-5cm-medium.jpg');
   grayIm{i}=rgb2gray(orImage{i});
   MedianIm{i}=medfilt2(grayIm{i},[5,5]);
   edge{i}=abs(imfilter(MedianIm{i},Hx))+abs(imfilter(MedianIm{i},Hy));
   binaryIm{i,1}=im2bw(edge{i},0.2*graythresh(edge{i}));
   L1=bwlabel(binaryIm{i,1});
   stat1=regionprops(binaryIm{i,1},'Area');
   area=cat(1,stat1.Area);
   v1=find(area>200);
   binaryIm{i,2}=ismember(L1,v1);
   L2=bwlabel(binaryIm{i,2});
   stat2=regionprops(binaryIm{i,2},'Orientation');
   orientation=cat(1,stat2.Orientation);
   v2=find(abs(orientation)<89 & abs(orientation)>1);
   binaryIm{i,3}=ismember(L2,v2);
   binaryIm{i,4}=bwmorph(binaryIm{i,3},'majority',200);
   binaryIm{i,5}=bwareaopen(binaryIm{i,4},50);
   [~,s,v]=rgb2hsv(orImage{i});
   tempS=s(binaryIm{i,5});
   if isempty(tempS)==0
     level=(min(tempS)+std(tempS));
     tempIm1=s.*binaryIm{i,5};
     binaryIm{i,6}=im2bw(tempIm1,level);
   else binaryIm{i,6}=binaryIm{i,5};
   end
   tempIm2=orImage{i};
   R=tempIm2(:,:,1);
   NR=R;
   G=tempIm2(:,:,2);
```

```
NG=G;
B=tempIm2(:,:,3);
NB=B;
NR(binaryIm{i,6})=255;
NG(binaryIm{i,6})=0;
NB(binaryIm{i,6})=0;
tempIm2(:,:,1)=NR;
tempIm2(:,:,2)=NG;
tempIm2(:,:,3)=NB;
RecIm{i}=tempIm2;
binaryIm{i,7}=bwmorph( binaryIm{i,6},'skel',inf);
Cracks_L{i}=size(find(binaryIm{i,7}),1);
value=Cracks_L{i};
RecIm{i}=insertText(RecIm{i},position,value,'AnchorPoint','Lefttop','FontSize',40);
h=figure(i);
%    set(h,'visible','off');
subplot(3,3,1)
imshow(grayIm{i})
title('Grayscale Image', 'fontsize',6)
subplot(3,3,2)
imshow(MedianIm{i})
title('Median Filtered', 'fontsize',6)
subplot(3,3,3)
imshow(edge{i})
title('Edge Image', 'fontsize',6)
subplot(3,3,4)
imshow( binaryIm{i,1})
title('Threshold Image', 'fontsize',6)
subplot(3,3,5)
imshow(binaryIm{i,2})
title('Post-Processed Image 1', 'fontsize',6)
subplot(3,3,6)
imshow( binaryIm{i,3})
title('Post-Processed Image 2', 'fontsize',6)
subplot(3,3,7)
```

```
    imshow( binaryIm{i,4})
    title('Post-Processed Image 3', 'fontsize',6)
    subplot(3,3,8)
    imshow( binaryIm{i,5})
    title('Post-Processed Image 4', 'fontsize',6, 'fontsize',6)
    subplot(3,3,9)
    imshow( binaryIm{i,6})
    title('Post-Processed Image 5', 'fontsize',6)
    filename=['Oldversion.' num2str(i) '.jpeg'];
    saveas(h,fullfile('C:\NDS\output',filename));
    h2=figure;
%     set(h2, 'visible', 'off');
    subplot(1,3,1)
    imshow(orImage{i})
    title('Original Color Image','fontsize',5.5)
    subplot(1,3,2)
    imshow(binaryIm{i,6})
    title('Detected Cracks Using Proposed Method','fontsize',5.5)
    subplot(1,3,3)
    imshow(RecIm{i})
    title('Reconstructed Image with Cracks and Statistics','fontsize',5.5)
    filename=['Output2.' num2str(i) '.jpeg'];
    saveas(h2,fullfile('C:\NDS\output',filename));
end
pause;
%%%% paper
approach%%%%%%%%%%%%%%%%%%%%%%%%%%%%%%%%%%%%%%%%%%%%%%%%%
%%%%%%%%%%
for i=1:NF
    paper_ap{i,1}=rgb2gray(orImage{i});
    paper_ap{i,2}=abs(imfilter(paper_ap{i,1},Hx))+abs(imfilter(paper_ap{i,1},Hy));
    paper_ap{i,3}=im2bw(paper_ap{i,2},graythresh(paper_ap{i,2}));
    paper_stat=regionprops(paper_ap{i,3},'Area');

    paper_area=cat(1,paper_stat.Area);
```

```
    paper_L=bwlabel(paper_ap{i,3});


    paper_v1=find(area>30);


    paper_ap{i,4}=ismember(paper_L,paper_v1);


    paper_ap{i,5}=bwmorph(paper_ap{i,4},'skel');


    paper_temp=orImage{i};


    paper_cracksL(i)=size(find(paper_ap{i,5}),1);


    paper_R=paper_temp(:,:,1);
    paper_G=paper_temp(:,:,2);
    paper_B=paper_temp(:,:,3);


    paper_R(paper_ap{i,4})=0;
    paper_G(paper_ap{i,4})=0;
    paper_B(paper_ap{i,4})=255;


    paper_temp(:,:,1)=paper_R;
    paper_temp(:,:,2)=paper_G;
    paper_temp(:,:,3)=paper_B;


    paper_ap{i,6}=paper_temp;


    paper_value=paper_cracksL(i);


paper_ap{i,7}=insertText(paper_ap{i,6},position,paper_value,'AnchorPoint','Lefttop','FontSize',40
);


    h3=figure;
    set(h3, 'visible', 'off');
```

```
subplot(2,2,1)
imshow( paper_ap{i,1})
title('Grayscale Image','fontsize',6)
subplot(2,2,2)
imshow(paper_ap{i,2})
title('Edge Image (Talab)','fontsize',6)
subplot(2,2,3)
imshow(paper_ap{i,3})
title('Threshold Image (Talab)','fontsize',6)
subplot(2,2,4)
imshow(paper_ap{i,4})
title('Post-Processed Threshold Image (Talab)','fontsize',6)
filename=['Paper.' num2str(i) '.jpeg'];
saveas(h3,fullfile('C:\NDS\output',filename));
h4=figure;
set(h4, 'visible', 'off');
subplot(1,3,1)
imshow(orImage{i})
title('Original Color Image (Talab)','fontsize',5)
subplot(1,3,2)
imshow(paper_ap{i,3})
title('Detected Cracks Using Talab Method (Talab)','fontsize',5)
subplot(1,3,3)
imshow(paper_ap{i,7})
title('Reconstructed Image with Cracks and Statistics (Talab)','fontsize',5)
filename=['paper2.' num2str(i) '.jpeg'];
saveas(h4,fullfile('C:\NDS\output',filename));

h5=figure;
set(h5, 'visible', 'off');
subplot(1,3,1)
imshow(orImage{i})
title('Original Color Image','fontsize',5)
subplot(1,3,2)
imshow(paper_ap{i,7})
```

```
title('Reconstructed Image Using Talab Method','fontsize',5)
subplot(1,3,3)
imshow(RecIm{i})
title('Reconstructed Image Using Proposed Method','fontsize',5)
filename=['Compare.' num2str(i) '.jpeg'];
saveas(h5,fullfile('C:\NDS\output',filename));

end
% End
```

Appendix C
Fatigue Crack Detection Code

```
clc

clear

close all

%% SPATIAL DOMAIN

%% IMAGE READING

file = dir('E:\FCI\*.jpg') ;

n = length (file) ;

H_gaussian = ghpf (2592,4608, 300, 300) ;

H_butter=bhpf(2592,4608,4,300);

for k = 1:n

    im_name  = file(k).name ;

    im1 = imread (fullfile ('E:\FCI\', file(k).name)) ;

    im = double(rgb2gray (im1)) ;


    %%  IMAGE ENHANCEMENT

    im_eq = histeq ( im ) ;

    im_av = medfilt2 (im, [6,6]) ;

    %% Sobel

    so = fspecial ('sobel') ;

    ed_sobel =  hypot (imfilter (im, so),imfilter (im ,so')) ;

    [bw_sobel, T_sobel] = edge ( ed_sobel, 'sobel');

    bw_sobel = ed_sobel >= (mean (ed_sobel(:))+ 3*std (ed_sobel (:))) ;

%    bw_sobel = bwareaopen (bw_sobel, 50) ;
```

```matlab
figure

imshow (ed_sobel,[])

title (file(k).name)

%% Canny

bw_canny = edge ( ed_sobel, 'canny') ;

bw_canny = bwareaopen ( bw_canny, 50) ;

figure,

imshow (bw_canny)

title (file(k).name)

%%LoG

loG = fspecial ('log', 20 , 2) ;

ed_log = imfilter (im, loG) ;

%    bw_log = edge ( ed_log, 'log') ;

bw_log = ed_log >= mean ((ed_log(:)) +  std (ed_log (:))) ;

bw_log = bwareaopen (bw_log, 200) ;

figure

imshow (ed_log,[])

title (file(k).name)

figure

imshow (bw_log)


%% Roberts

Rx = [1 0; 0 -1];

ed_ro =  hypot (imfilter (im, Rx),imfilter (im,Rx')) ;
```

```
    bw_ro = edge (ed_ro, 'roberts') ;

    bw_ro = ed_ro >= mean ((ed_ro(:)) + 3* std (ed_ro(:))) ;

    bw_ro = bwareaopen ( bw_ro, 50 ) ;
%
    figure,

    imshow (bw_ro)

    title ( file(k).name)
%
    %% FREQUENCY DOMAIN

    [r,c] = size (im) ;


    im_fft = fftshift ( fft2 ( im)) ;


    figure
    mesh (H_butter)
    grid off


    figure
    mesh (H_gaussian)
    grid off
%
    H_butter=bhpf(r,c,4,300);

    im_fft_but = H_butter.* im_fft ;

    ed_butter = ifft2 (ifftshift ( im_fft_but)) ;


    bw_butter = ed_butter <=-10 ;
    bw_butter = bwareaopen ( bw_butter, 50) ;

    figure

    imshow ( bw_butter)
    title (file(k).name)



    im_fft_gau = H_gaussian.* im_fft ;
```

```
ed_gaussian = ifft2 ( ifftshift ( im_fft_gau)) ;

bw_gaussian = ed_gaussian <= -10 ;

bw_gaussian = bwareaopen ( bw_gaussian, 50 ) ;

figure

imshow ( bw_gaussian)

title (file(k).name)

R = im1 (:,:,1) ;
B = im1 (:,:,2) ;
G = im1 (:,:,2) ;
B = im1 (:,:,3) ;
R (bw_log) = 0 ;
G (bw_log) = 0 ;
B (bw_log) = 255 ;
im2= im1 ;
im2 (: ,:,1) = R;
im2 (: ,:,2) = G;
im2 (: ,:,3) = B;
figure, imshow (im2)

end
```